UNIVERSITY OF OKLAHOMA

GRADUATE COLLEGE

STABLE NITROGEN ISOTOPE SIGNAL IN CRUDE OILS THROUGHOUT GEOLOGIC TIME

A THESIS

SUBMITTED TO THE GRADUATE FACULTY

in partial fulfillment of the requirements for the

Degree of

MASTER OF SCIENCE

By

ALYSE JOHANSEN
Norman, Oklahoma
2017

Downloaded from SHAREOK. Persistent Handle URL: https://hdl.handle.net/11244/50768

STABLE NITROGEN ISOTOPE SIGNAL IN CRUDE OILS THROUGHOUT GEOLOGIC TIME

A THESIS APPROVED FOR THE
CONOCOPHILLIPS SCHOOL OF GEOLOGY AND GEOPHYSICS

BY

_____
Dr. Michael H. Engel, Chair

_____
Dr. R. Douglas Elmore

_____
Dr. John E. Zumberge

© Copyright by ALYSE JOHANSEN 2017
All Rights Reserved.

In dedication to my husband, Zachary Johansen, my rock.

Acknowledgements

To Dr. Michael Engel, for awarding me this amazing opportunity in attaining my Master's degree at the University of Oklahoma under your advisement. Thank you for your never-ending patience, your guidance and care. I would not be here without you.

To my other committee members, Dr. Douglas Elmore and Dr. John Zumberge. I appreciate all of Dr. Elmore's care in teaching me and taking the time to help me understand geological processes. I want to thank Dr. Zumberge and GeoMark for providing the oil samples used in this research and for taking the time to be on my thesis committee.

To Rick Maynard, thank you for all the time you put into running my samples. I appreciate all your hard work and the many hours spent. Also to Sarah Engel, I appreciate your patience and time in teaching me column chromatography and molecular sieving.

To my mom and grandma, Elissa Maughan and LaRey West, you encouraged me and always believed in me. Also to my brother Tyler Maughan, thank you for supporting me and helping me so much along the way.

I want to thank all my geology friends. You have cared for me so much during these two years. Thank you for teaching me and helping me in my classes, and in life in general.

Table of Contents

Acknowledgements iv

List of Tables vii

List of Figures viii

Abstract x

Introduction 1

Sample Selection … 7

Experimental Methods……...9

Sample Preparation 9

Column Chromatography 9

Nitrogen Isotope Analysis…….10

Calculation of Delta……...10

Results…….12

The Stable Nitrogen Isotopic Analysis of Mexican Oils……..12

The Stable Nitrogen Isotopic Analysis of Middle East Oils……16

The Stable Nitrogen Isotopic Analysis of the Sixty-two Crude Oils ……..19

Discussion……27

The $\delta^{15}N$ values of the Mexican Oils……...27

The $\delta^{15}N$ values of the Middle East Oils…….34

The $\delta^{15}N$ values of the Sixty-two Crude Oils ……..36

Conclusion ……..47

References 49

Appendix 1: Age, lithology, and sample location ……..57

Appendix 2: Age and $\delta^{15}N$ values for each oil sample……60

List of Tables

Table 1. Mexican oils of increasing maturity……8

Table 2. Middle East oils of increasing maturity……...……...8

Table 3. Maturity parameters and $\delta^{15}N$ values for the Mexican oils……...12

Table 4. Maturity parameters and $\delta^{15}N$ values for the Middle East oils…….12

Table 5. Depositional environment parameters for the Mexican oils…….32

Table 6. Depositional environment parameters for the Middle East oils……34

List of Figures

Figure 1. Nitrogen cycle in the open ocean…….....3

Figure 2. Graphical representation of $\delta^{15}N$ values for varying redox conditions……....5

Figure 3. The $\delta^{15}N$ NSO values of the Mexican oils …….....13

Figure 4. The $\delta^{15}N$ asphaltene values of the Mexican oils…….....14

Figure 5. The combined $\delta^{15}N$ NSO and asphaltene values of the Mexican oils ……....15

Figure 6. The $\delta^{15}N$ NSO values of the Middle East oils…….16

Figure 7. The $\delta^{15}N$ asphaltene values of the Middle East oils……17

Figure 8. The combined $\delta^{15}N$ NSO and asphaltene values of the Middle East oils……18

Figure 9. The $\delta^{15}N$ NSO values of siliciclastic derived oils…….....19

Figure 10. The $\delta^{15}N$ asphaltene values of siliciclastic derived oils…….20

Figure 11. The $\delta^{15}N$ NSO values of carbonate/marl derived oils……21

Figure 12. The $\delta^{15}N$ asphaltene values of carbonate/marl derived oils……...21

Figure 13. NSO and asphaltene values of lacustrine/hypersaline derived oils……....22

Figure 14. The combined $\delta^{15}N$ NSO values for all sixty-two oils……..23

Figure 15. The combined $\delta^{15}N$ asphaltene values for all sixty-two oils……..24

Figure 16. The combined $\delta^{15}N$ NSO and asphaltene values for all sixty-two oils……..26

Figure 17. Chromatogram of sample 22……..29

Figure 18. Chromatogram of sample 33……..30

Figure 19. Chromatogram of sample 31……..30

Figure 20. Chromatogram of sample 32……..30

Figure 21. Chromatogram of sample 30……..30

Figure 22. NSO and asphaltene values for all sixty-two oils with kerogen values…….37

Figure 23. High resolution of Upper Mississippian to Middle Triassic $\delta^{15}N$ values.....41

Abstract

Stable nitrogen isotopic compositions of asphaltene and NSO hydrocarbon fractions from sixty-two crude oils derived from siliciclastic, carbonate/marl, hypersaline and lacustrine source rocks of known geologic age ranging from the Precambrian/ Cambrian to the Neogene were analyzed to determine whether the stable nitrogen isotope composition of crude oils record the secular change for $\delta^{15}N$ that have been observed for kerogen and sedimentary organic matter (e.g. Stüeken et al., 2015 and references therein). The stable nitrogen isotope compositions of the sixty-two crude oils appear to correlate well with the kerogen and sedimentary organic matter from the literature. In addition, two trends in enrichments in ^{15}N are observed for the Carboniferous/Permian and in the Miocene, resulting from incomplete denitrification. Three shifts in depletion in ^{15}N are also observed in the Cambrian/Ordovician, Silurian/Devonian, and the Triassic through the Paleogene. The Cambrian/Ordovician depletion is thought to result from more oxic ocean waters driving nitrification and assimilation. The Silurian/Devonian, and the Triassic through the Paleogene depletions are thought to derive from anoxic ocean waters driving nitrogen fixation. Enrichments and depletions in ^{15}N were independent of source rock type. Within the sixty-two crude oils, another study was conducted on 5 marine carbonate oils from Mexico and 4 marine carbonate oils from Middle East to determine the effects of thermal maturity on the stable nitrogen isotope composition of these oils. There was no systematic increase in $\delta^{15}N$ values with increasing thermal maturity observed.

Introduction

Nitrogen is essential for life, and is present in proteins and amino acids, purines and pyrimidines. Nitrogen is the fourth most abundant element in the biomass (Canfield et al., 2010; Godfrey & Glass, 2011; Galbraith et al, 2013; Stüeken et al., 2015). Nitrogen is a central component in marine ecosystems and limits the growth of marine life throughout most of the oceans (Francis et al., 2005; Canfield et al., 2010; Tesdal et al., 2013). Therefore, nitrogen is representative of the biochemical processes in the world's oceans, past and present (Sigman & Casciotti, 2001).

Nitrogen has two stable isotopes, ^{14}N (99.64%) and ^{15}N (0.36%), with molecular nitrogen (N_2) in the Earth's atmosphere and oceans accounting for over 99% of the total nitrogen on Earth (e.g. Hoefs, 2015). Fractionation between these two isotopes is caused by physical, chemical and biological mechanisms (Sigman & Casciotti, 2001). Nitrogen isotope fractionation can be preserved in kerogen throughout geologic time (e.g. Macko & Quick, 1986; Altabet & Francois, 1994; Quan et al., 2013; Stüeken et al., 2015). Previous studies have shown that crude oils generally preserve the stable carbon isotope compositions of the kerogens from which they were derived (e.g. Andrusevich et al., 1998 and references therein). Similarly, preliminary results indicate that the stable sulfur isotope compositions of crude oils also reflect that of the kerogens from which they were derived (e.g. Engel and Zumberge, 2007 and references therein). It is hypothesized that the $\delta^{15}N$ value of crude oils will also reflect that of the kerogens from which the crude oils are derived, which in turn will reflect the stable nitrogen isotope composition of the biomass from which the kerogens were derived.

The marine nitrogen cycle (Figure 1) consists of several steps, the most important being nitrogen fixation, nitrification and denitrification/anammox reactions that are biologically mediated and convert nitrogen between a wide range of redox states (Sigman & Casciotti, 2001; Altabet, 2005; Quan et al., 2013). Molecular nitrogen enters the ocean by diffusion from the atmosphere, microbial N_2 fixation, and from weathering of the continents (Sigman & Casciotti, 2001; Meckler et al., 2011). Oceanic sink processes are denitrification and anammox (Junium and Arthur, 2007; Meckler, et al., 2011 Galbraith et al., 2013).

During the nitrogen cycle in the ocean, most organisms, although readily accessible, cannot directly use molecular nitrogen. As molecular nitrogen enters the ocean, nitrogen fixing bacteria with the help of an enzyme, Nitrogenase, convert N_2 into nitrate, an essential nutrient for marine phytoplankton. A series of microbial mediated steps are involved in the conversion of organic nitrogen back to nitrite and nitrate, some of which is cycled back into biomass via photosynthesis. When oxygen falls to less than 5 micromolar (μM), many bacteria find it more efficient to convert organic nitrogen back to N_2 by denitrification which respires organic matter with nitrate (NO_3^-) as an electron acceptor. (e.g., Sigman & Casciotti, 2001; Altabet, 2005; Godfrey & Glass, 2011; Meckler et al., 2011). Anammox, like denitrification, is present in the water column at low oxygen concentrations and converts organic nitrogen back to N_2 through the reaction between ammonium (NH_4) and nitrite (NO_2) to produce N_2 and water (Devol, 2008 and references therein).

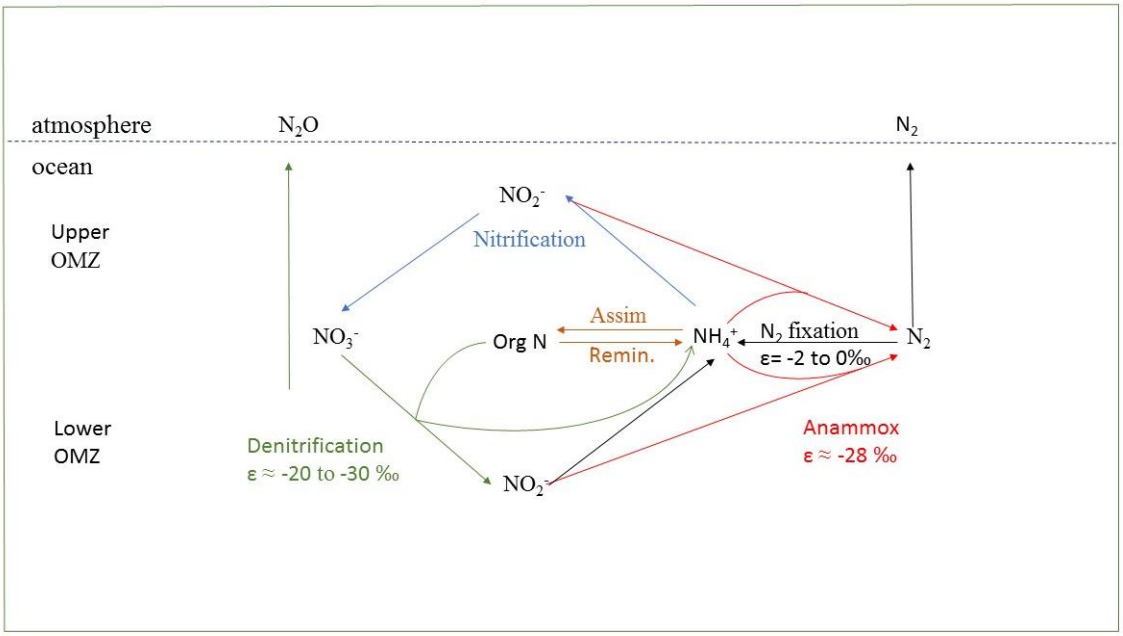

Figure 1. Nitrogen cycle in the open ocean. Molecular nitrogen is sourced to the ocean through the atmosphere, microbial N_2 fixation, and from weathering of the continents. Oceanic sinks include denitrification and anammox process that convert organic nitrogen back to N_2. Modified after Lam et al., 2009.

Several processes in the nitrogen cycle can preferentially remove or take up ^{15}N or ^{14}N, changing the $^{15}N/^{14}N$ ratios (e.g., Sigman & Casciotti, 2001; Godfrey & Glass, 2011). During the microbial process of N_2-fixation, little fractionation is observed, resulting in $\delta^{15}N$ values of newly fixed nitrogen of -2 to 0‰, close to the observed value of 0.0‰ for molecular nitrogen in the Earth's past and present-day atmosphere (Meckler et al., 2011; Kritee et al., 2012 and references therein; Marty et al., 2013). With denitrification, a strong, negative isotope fractionation of -20 to -30‰ is generally observed for N_2 (Sigman & Casciotti, 2001; Altabet, 2005), as denitrification preferentially removes the ^{14}N isotope, leaving the heavy ^{15}N isotope behind, enriching the residual nitrate (Altabet, 2005; Meckler et al., 2011). Based on recent culture experiments by Kritee et al. (2012), a range of $\delta^{15}N$ values from -10 to -15‰ may be

more representative of the environment in the ocean. However, a range of -25 to -30‰ is what has actually been measured in the field (Kern et al., 2016). Anammox is still a relatively recently (Mulder et al., 1995) discovered microbial pathway (Godfrey & Glass, 2011) and its potential impact on the stable nitrogen isotope cycle in ocean waters over geologic time is not known. However, recent batch culture experiments report a wide range of nitrogen isotope effects caused by anammox bacteria under varied growth conditions which appear to be similar to denitrification (Brunner et al., 2013), yet these nitrogen isotope effects are still uncertain in the natural world (Wenk, 2013). Anammox processes are, therefore, commonly included under denitrification (Rivera et al., 2015).

Denitrification is the main process in suboxic conditions where there is enough oxygen in the water column to support the production of nitrate, but the oxygen concentration cannot be too high or the enzymes needed to convert nitrate to N_2 are inhibited. The denitrification reaction is generally characterized by higher $\delta^{15}N$ values. When conditions are fully anoxic, nitrate is unstable. The denitrification reaction goes to completion and no measurable isotopic fractionation is preserved. Both denitrification and nitrification are less dominant processes in anoxic environments than the nitrogen fixation process (Quan et al., 2013). Therefore, a decrease in $\delta^{15}N$ values from a suboxic to anoxic environment is observed due to small isotope fractionation associated with nitrogen fixation (Figure 2). Fully oxic conditions also inhibit denitrification. Fully oxic water column conditions are dominated by nitrification and nitrogen uptake processes. As with nitrogen fixation, nitrification has a small isotope

fractionation factor and again a decrease in $\delta^{15}N$ values from suboxic to oxic environments is observed (Figure 2); (Quan et al., 2013; Rivera et al., 2015).

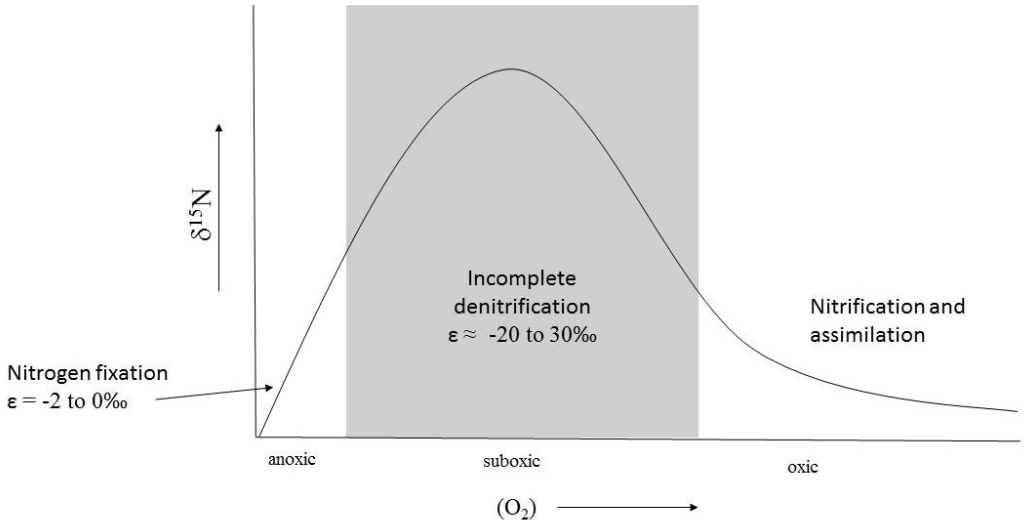

Figure 2. Graphical representation of bulk sediment $\delta^{15}N$ values and water oxygen concentrations. The $\delta^{15}N$ values are highest in the suboxic zone where incomplete denitrification is the dominate nitrogen process and is associated with large isotope fractionation that enriches the substrate by 20-30‰ (Altabet, 2005). A move to more anoxic waters lowers $\delta^{15}N$ values as nitrogen fixation becomes the primary process and is associated with little isotope fractionation. A move to more oxic water will again lower the $\delta^{15}N$ value from the suboxic zone, as nitrification is the primary nitrogen process and like nitrogen fixation has a small isotope fractionation factor. Modified after Rivera et al., 2015.

The signal of nitrogen isotopes in sedimentary organic matter can improve our understanding of the past nitrogen cycle (Junium and Arthur, 2007; Godfrey & Glass, 2011; Tesdal et al., 2013; Saitoh et al., 2014) and be used to determine past biochemical cycling in the paleo-oceanographic record (Altabet & Francois, 1994; Lehmann et al., 2002; Robinson et al., 2012; Galbraith et al., 2013). Stable nitrogen isotope values can also be used to help distinguish crude oils derived from different source rocks and to differentiate types of organic matter (Macko & Quick, 1986; Williams et al., 1995; Marcano et al., 2013). Finally, because the reactions responsible for the conversion

between different nitrogen forms are strongly influenced by the redox state of the water column, nitrogen isotopes can be used to characterize depositional environments (Rivera et al., 2015 and references therein).

The use of stable nitrogen isotopes to reconstruct paleo-environments relies on the preservation of the primary nitrogen isotopic signal (Godfrey & Glass, 2011; Quan et al., 2013). However, these primary signals may, to some extent, be altered during burial, diagenesis (Robinson et al., 2012; Tesdal et al., 2013; Rivera et al., 2015), catagenesis, thermal maturity, and fluid heat flow (Quan et al., 2013; Rivera et al., 2015).

This study further investigates secular change in the ocean water nitrogen cycle using the stable nitrogen isotope composition of crude oils. Previous studies have documented that the stable isotope compositions of crude oils reflect that of the source rocks from which they were derived, in particular for carbon (e.g. Andrusevich et al., 1998) and sulfur (e.g. Engel and Zumberge, 2007). In the present study, it will be determined whether the stable nitrogen isotope composition of crude oils also record the secular change for $\delta^{15}N$ that have been observed for kerogen and sedimentary organic matter (e.g. Stüeken et al., 2015 and references therein).

Sample Selection

Sixty-two crude oils derived from siliciclastic, carbonate/marl, hypersaline and lacustrine source rocks of known geologic age ranging from the Precambrian/ Cambrian to the Neogene were obtained from the sample collection of GeoMark Research, Inc., Houston, TX (Appendix 1). The geologic ages of the source rocks of these oils were previously determined using biomarker analyses. Differences in the depositional environment were used to determine effects on the biomass and whether the fluctuation in the nitrogen isotope signal is global or specific to certain environments. The numbers used in the text, tables, and figures correspond to the oil identification numbers listed in Appendix 1.

Within the sixty-two-crude oil set, five oils (22, 33, 31, 32, and 30) were selected from the Sureste Basin and Tampico Basin in Mexico (Table 1) and four oils (21, 27, 26, and 25) were selected from the Central Arabian Province Basin in the Middle East (Table 2) to determine the effects of thermal maturity on the stable nitrogen isotope composition of these oils. The oils selected from Mexico are of increasing API gravity, ranging from 12.8 to 32.6, and based on Ts/Tm values were of increasing maturity (Table 1). The oils selected from the Middle East are also of increasing API gravity, ranging from 27.0 to 33.2 and were also of increasing maturity (Table 2).

Table 1
Mexican oils of increasing maturity

Sample ID	Basin	API Gravity	C27 Ts/Tm	C29 Ts/Tm
22	Tampico	12.8	0.37	0.12
33	Sureste	15.0	0.30	0.09
31	Sureste	18.1	0.74	0.20
32	Sureste	31.9	0.81	0.24
30	Sureste	32.6	1.04	0.28

Table 2
Middle East oils of increasing maturity

Sample ID	Basin	API Gravity	C27 Ts/Tm	C29 Ts/Tm
21	Central Arabian Province	27.0	0.50	0.17
27	Central Arabian Province	31.7	1.38	0.28
26	Central Arabian Province	32.9	1.20	0.23
25	Central Arabian Province	33.2	2.84	0.41

Experimental Methods

Sample Preparation

Because of the small abundance of nitrogen in crude oils, nitrogen isotope analysis focused on the asphaltene and NSO fractions of each crude oil that were recovered by deasphalting the crude oil and column chromatography of the remaining maltene fractions. Approximately 100 mg of each whole crude oil was placed in a 35-ml vial and weighed. Each oil was then topped under N_2 in a heating block at approximately 80°C for 45 minutes. The vials were then re-weighed to determine the percent of volatiles. The samples were then deasphalted in approximately 30 ml of hexane at room temperature and left overnight. The samples were then centrifuged to isolate the asphaltenes. Because of low nitrogen abundance, deasphalting was preformed two or more times for each oil sample and the asphaltene fractions for each oil were combined. The remaining maltene fraction was pipetted out of the 35-ml vial and evaporated under N_2, and re-dissolved in approximately 1 ml of hexane in a new 35-ml vial.

Column Chromatography

The maltene fractions were separated on chromatographic columns with dimensions of 50 cm long, 11 mm inner diameter, and had a 250-ml reservoir. The chromatographic columns were first plugged with glass wool and sand and then slurry packed with 15 grams of silica gel in hexane. Prior to column packing, the silica gel was pre-heated to 300°C. The saturate, aromatic and NSO fractions were recovered from the column with 50 ml each of hexane, dichloromethane, and dichloromethane/ methanol (1:1 ratio), respectively. The fractions were then concentrated under N_2 or by

rotoevaporation. Because of low nitrogen abundance, column chromatography was performed two or more times on the same sample and the NSO fractions for each oil were combined (Andrusevich et al., 1998)

Nitrogen Isotope Analysis

Approximately 1-2 mg of each NSO and Asphaltene sample was weighed on a micro-balance and wrapped in tin capsules. The tin capsules were then placed in a Costech zero blank autosampler, which is mounted on a Costech 4010 elemental analyzer. The samples are purged with high purity helium to remove air and then analyzed by flash combustion. Flash combustion was achieved by injecting a large pulse of oxygen gas at the exact time of the sample drop. The resulting peak was carried by a helium stream at a flow rate of 100 ml/min to a Thermo Conflo III interface, which was connected to the ion source of a Thermo Delta V Plus isotope ratio mass spectrometer. The temperature of the quartz combustion column was 1,000°C, the copper reduction column was 650°C, and the gas chromatography (GC) column oven was 55°C. A large CO_2 absorbent trap was inserted in-between the water trap and the GC column to prevent interference from CO in the ion source. The signal peak, therefore, only consists of N_2. Samples were run multiple times to ensure that the $\delta^{15}N$ value for each oil was within an acceptable error of approximately ± 0.5‰.

Calculation of Delta

The $\delta^{15}N$ value of each sample was determined relative to atmospheric AIR as:

$$\delta^{15}N = ([R\ (^{15}N/^{14}N)_{P}/\ R\ (^{15}N/^{14}N)_{STD}] - 1) * 1000$$

where $R(^{15}N/^{14}N)_P = N(^{15}N)_P / N (^{14}N)_P$ which is the ratio of the number of ^{15}N atoms to the number of ^{14}N atoms in sample P and equivalent parameters apply for the AIR standard (Coplen, 2011). The raw $\delta^{15}N$ values of the samples were then processed by 2-point linear normalization (Paul et al., 2007) using the standards USGS-40 ($\delta^{15}N$ = -4.52‰) and USGS-41 ($\delta^{15}N$ = + 47.57‰), (Qi et al., 2003).

Results

The Stable Nitrogen Isotopic Analysis of the Mexican Oils

The $\delta^{15}N$ values for the NSO fractions and the asphaltene (Asp) fractions of the thermal maturity study of the Mexican oils and Middle Eastern oils are summarized in Tables 3 and 4, respectively. Graphical representations of the Mexican and Middle East oil compositions are also shown in below.

Table 3
Maturity parameters and $\delta^{15}N$ values for the Mexican oils

Sample ID	API Gravity	C27 Ts/Tm	C29 Ts/Tm	Number of Times Measured	$\delta^{15}N$ ‰ (NSO)	Number of Times Measured	$\delta^{15}N$ ‰ (Asp)
22	12.8	0.37	0.12	4	0.20 ±0.19	5	-0.80±0.23
33	15.0	0.30	0.09	6	-0.87±0.60	6	-0.92±0.42
31	18.1	0.74	0.20	3	0.65±0.97	3	-0.34±0.21
32	31.9	0.81	0.24	5	0.70±0.81	5	0.17±0.32
30	32.6	1.04	0.28	2	1.24±0.87	2	-0.70±0.61

Table 4
Maturity parameters and $\delta^{15}N$ values for the Middle East oils

Sample ID	API Gravity	C27 Ts/Tm	C29 Ts/Tm	Number of Times Measured	$\delta^{15}N$ ‰ (NSO)	Number of Times Measured	$\delta^{15}N$ ‰ (Asp)
21	27.0	0.50	0.17	4	0.59±1.13	4	0.51±0.82
27	31.7	1.38	0.28	3	0.59±0.50	4	1.46±0.33
26	32.9	1.20	0.23	3	1.91±0.64	4	2.40±0.44
25	33.2	2.84	0.41	4	1.20±0.61	3	2.20±0.41

The $\delta^{15}N$ values for the NSO fraction in the Mexican oils from the Tampico and Sureste basin show an enrichment in ^{15}N with increasing API gravity and range from -

0.87 to 1.24‰ (Figure 3). The asphaltene fraction in the Mexican oils also show an enrichment in ^{15}N with increasing API gravity in samples 33, 31, and 32, ranging from -0.92 to 0.17‰.

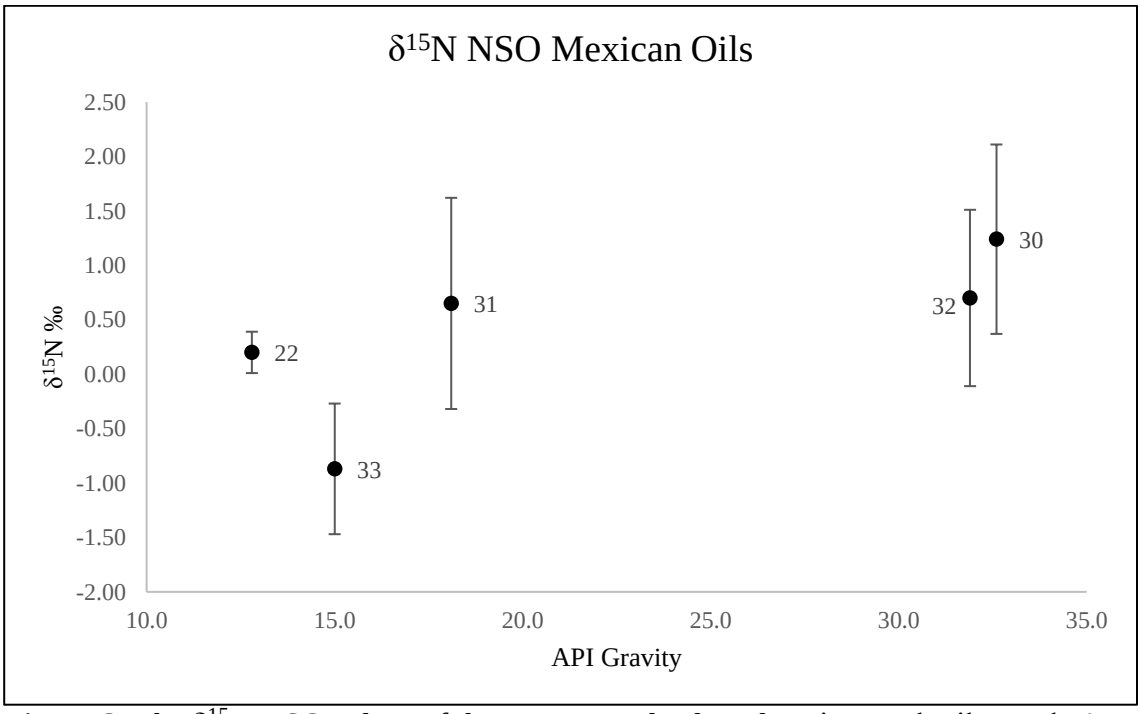

Figure 3. The $\delta^{15}N$ NSO values of the Mexican oils plotted against each oil samples' respective API gravity. Each point is labeled with corresponding ID from Table 1, and plotted with error bars to show each sample's standard deviation.

Sample 30 is depleted in ^{15}N in the asphaltene fraction relative to samples 31 and 32, with a value of -0.70‰ (Figure 4), despite having the highest API gravity. Sample 22 from the Tampico basin is enriched in ^{15}N in both the NSO and asphaltene fractions relative to sample 33, despite being the lowest in API gravity. Because sample 22 is from the Tampico basin there is some uncertainty whether the thermal maturity of sample 22 can be evaluated in relationship to the Sureste basin oils. To evaluate the effects of thermal maturity, an assumption is made that the organic matter from which the oils were derived is deposited under the same conditions and depositional environments (Rivera, 2013). Nitrogen isotopes are local indicators, as the nitrogen

cycle depends on water column conditions, and thus the $\delta^{15}N$ values may not be comparable between sites (Quan et al., 2013). Combined $\delta^{15}N$ values for the fractions of the Mexican oils are shown in Figure 5.

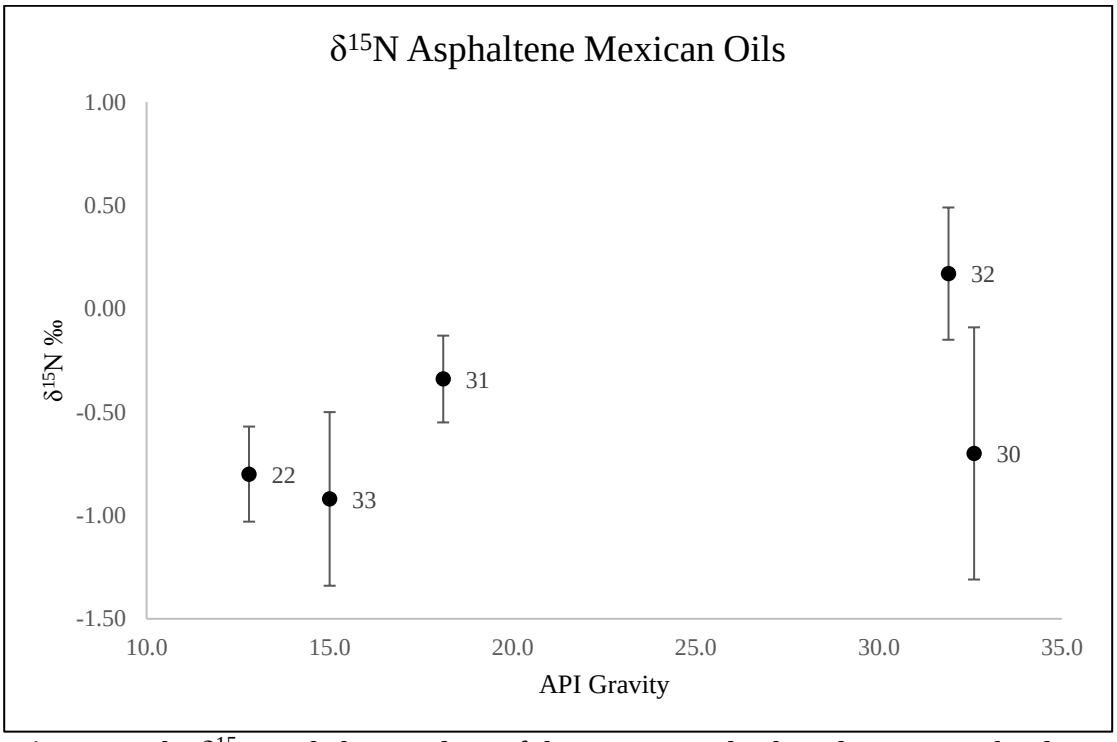

Figure 4. The $\delta^{15}N$ asphaltene values of the Mexican oils plotted against each oil samples' respective API gravity. Each point is labeled with corresponding ID from Table 1, and plotted with error bars to show each sample's standard deviation.

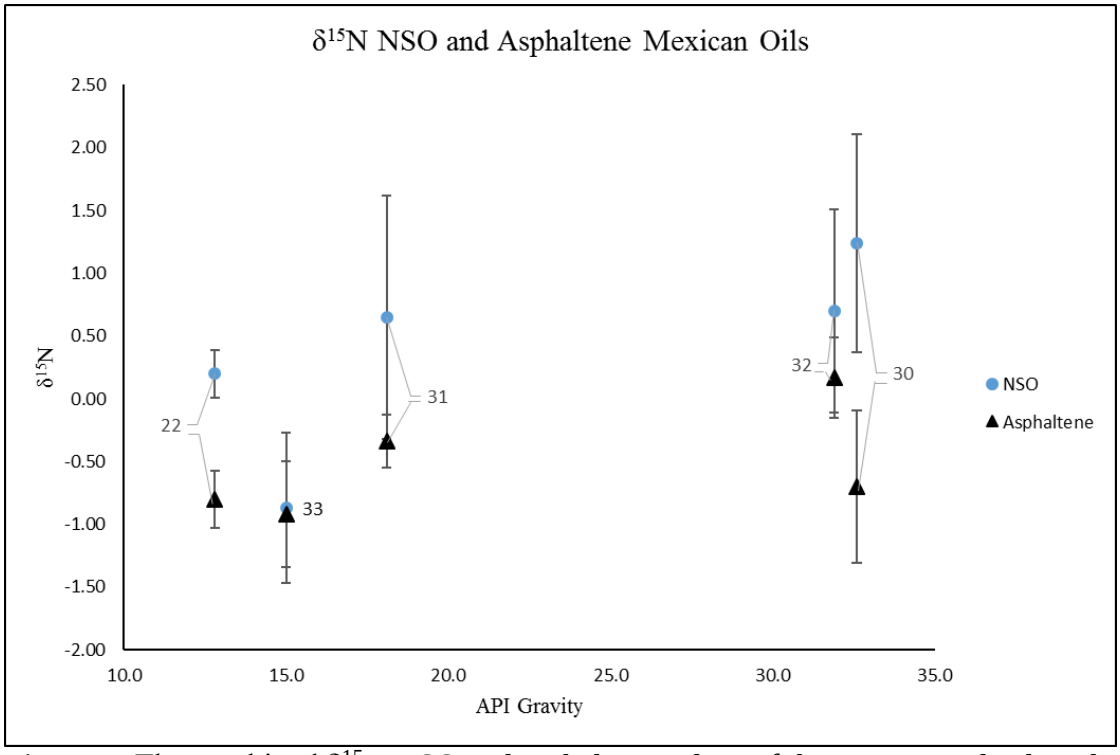

Figure 5. The combined $\delta^{15}N$ NSO and asphaltene values of the Mexican oils plotted against each oil samples' respective API gravity. Each point is labeled with corresponding ID from Table 1, and plotted with error bars for each fraction to show each sample's standard deviation.

The Stable Nitrogen Isotopic Analysis of the Middle East Oils

The $\delta^{15}N$ values for the NSO fractions in the Middle East oils from the Central Arabian Province basin show an enrichment in ^{15}N with increasing API gravity and range from 0.59 to 1.91‰ in samples 21, 27, and 26. Sample 25 was depleted in ^{15}N with a value of 1.20‰ compared with the $\delta^{15}N$ value for sample 26, despite sample 25 being of higher API gravity (Figure 6). The stable nitrogen isotopic compositions of the asphaltene fractions show an enrichment in ^{15}N with increasing API gravity and range from 0.51-2.40‰ for samples 21, 27 and 26. Again sample 25 is depleted in ^{15}N with a $\delta^{15}N$ value of 2.20‰ compared with that of sample 26 (Figure 7). A combined plot of NSO and asphaltene $\delta^{15}N$ values for the Middle Eastern oils is shown in Figure 8.

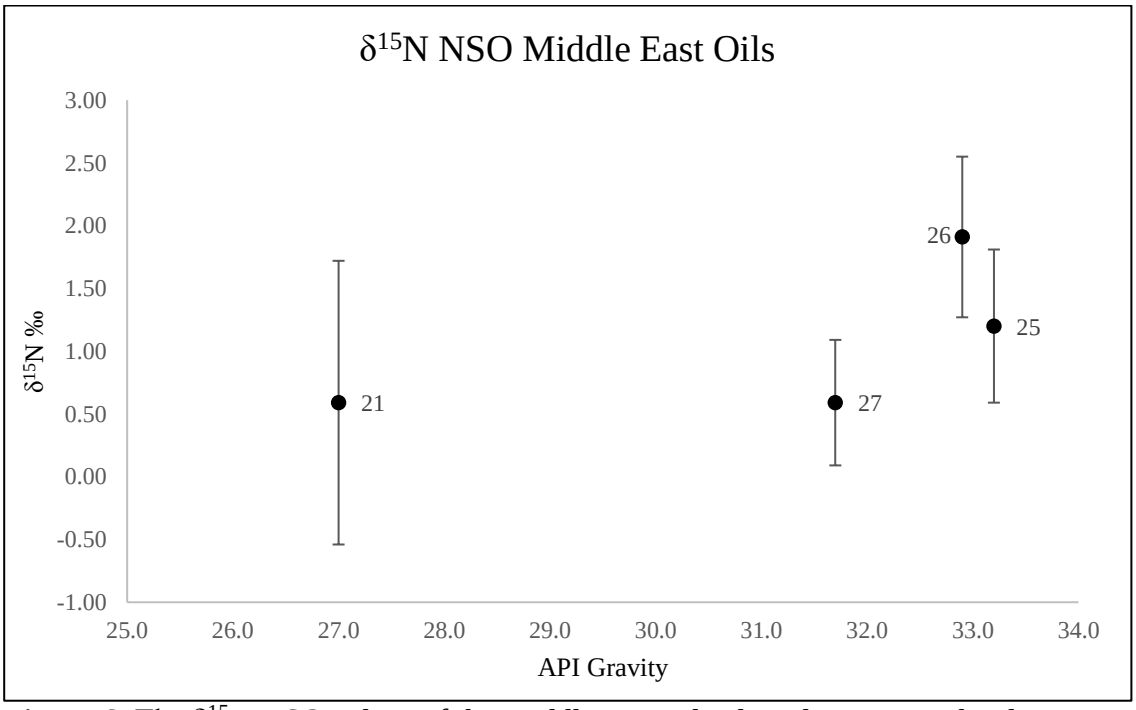

Figure 6. The $\delta^{15}N$ NSO values of the Middle East oils plotted against each oil samples' respective API gravity. Each point is labeled with corresponding ID from Table 2, and plotted with error bars to show each sample's standard deviation.

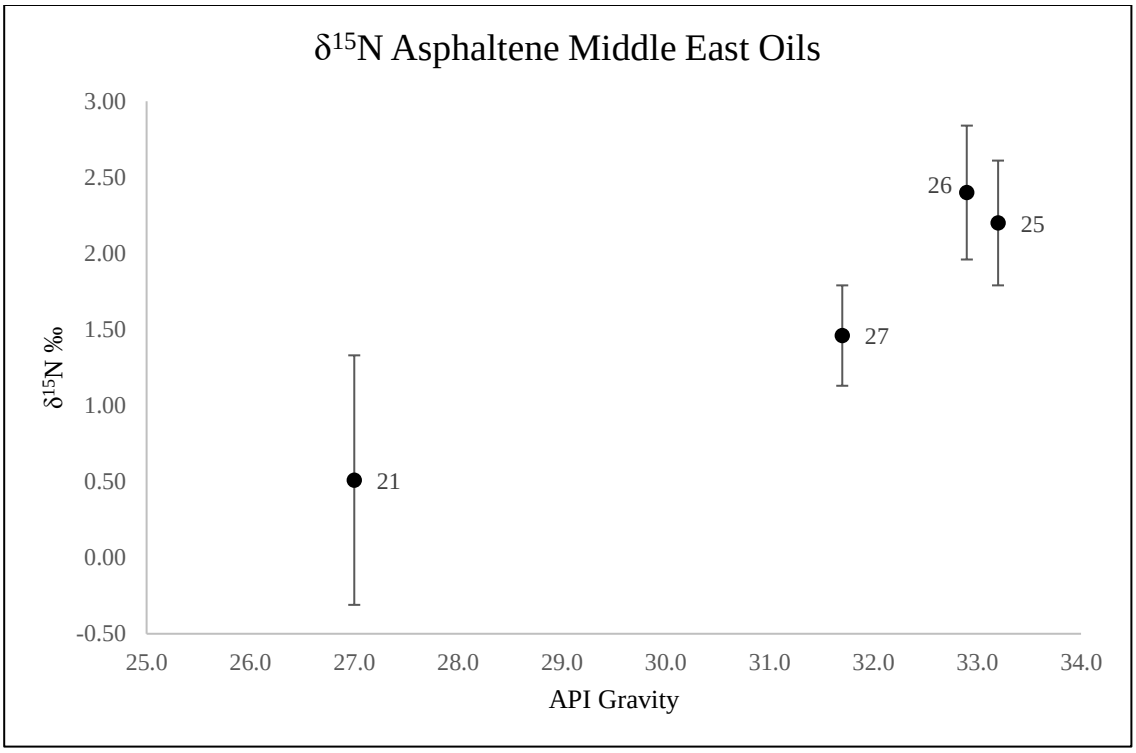

Figure 7. The $\delta^{15}N$ NSO values of the Middle East oils plotted against each oil samples' respective API gravity. Each point is labeled with corresponding ID from Table 2, and plotted with error bars to show each sample's standard deviation.

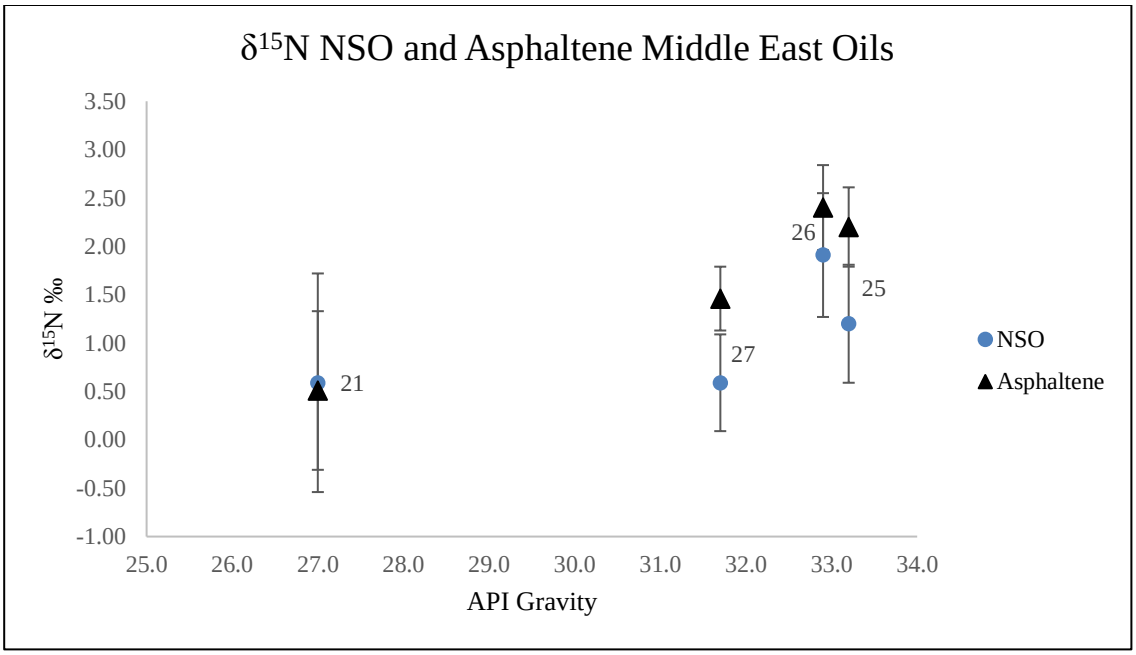

Figure 8. The combined $\delta^{15}N$ NSO and asphaltene values of the Middle East oils plotted against each oil samples' respective API gravity. Each point is labeled with corresponding ID from Table 2, and plotted with error bars to show each sample's standard deviation.

The Stable Nitrogen Isotopic Analysis of the sixty-two crude oils of Varying Geologic Age

The stable nitrogen isotopic compositions of the NSO fractions and the asphaltene fractions of the sixty-two crude oil samples are summarized in Appendix 2. The NSO $\delta^{15}N$ values of oils derived from siliciclastic source rocks is shown in Figure 9. The asphaltene $\delta^{15}N$ values of oils derived from siliciclastic source rocks is shown in Figure 10. The NSO and asphaltene fractions plot similarly. Also, note that three samples, numbers 50, 52, and 55 did not have an asphaltene fraction. Consequently, those data points are absent for the asphaltene graph (Figure 10).

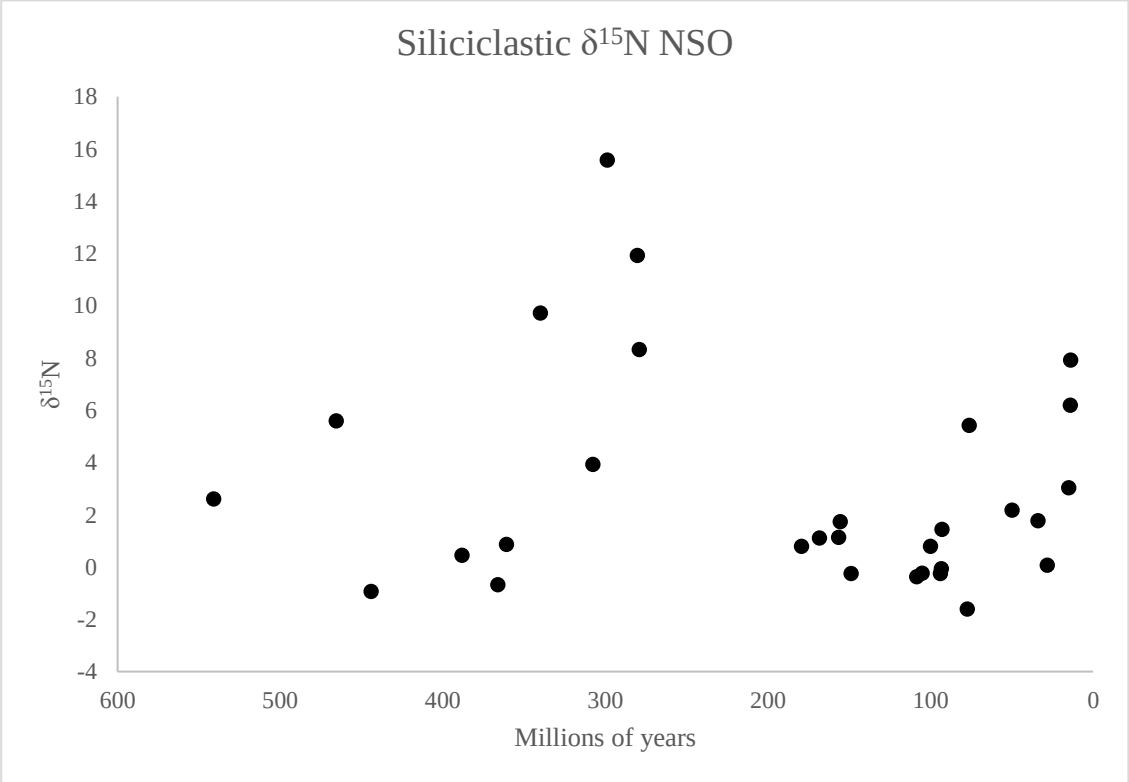

Figure 9. Oils derived from siliciclastic source rocks of the sixty-two crude oils NSO values plotted against each oil's geologic age.

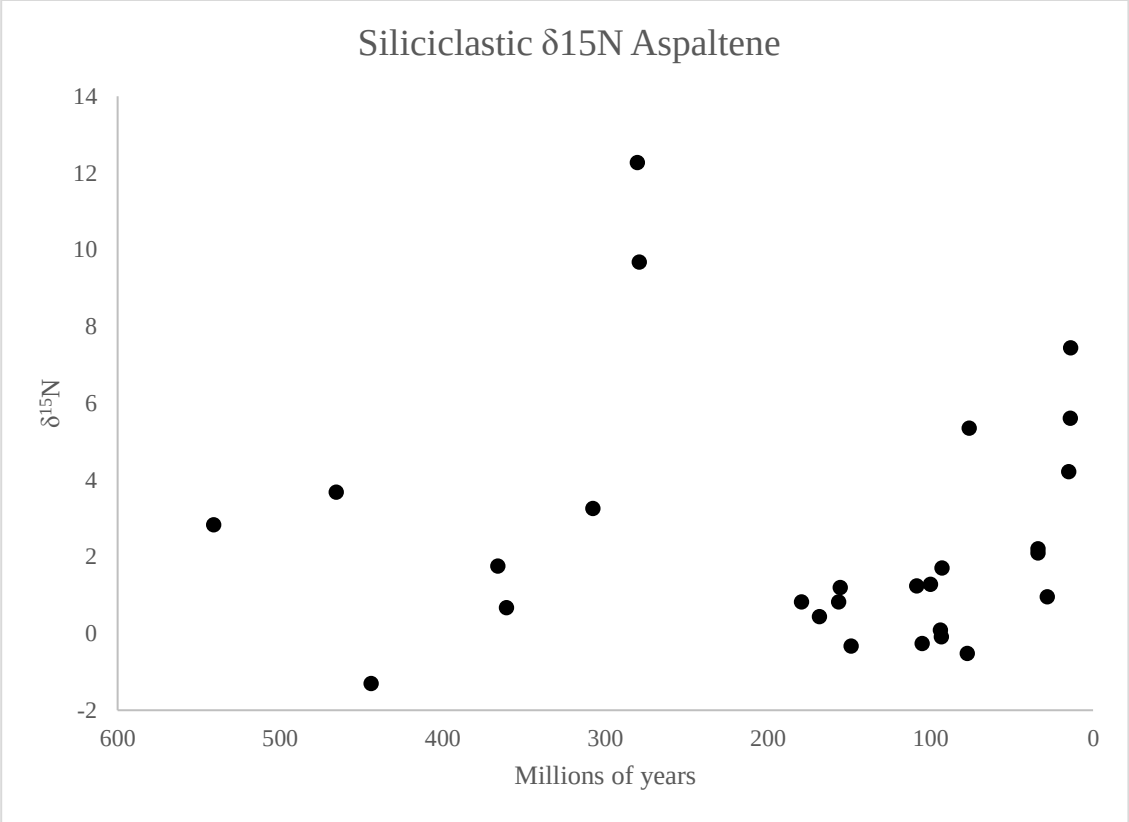

Figure 10. Oils derived from siliciclastic source rocks of the sixty-two crude oils asphaltene values plotted against each oil's geologic age.

The NSO $\delta^{15}N$ values of oils derived from carbonate/marl source rocks is shown in Figure 11. The asphaltene $\delta^{15}N$ values of oils derived from carbonate/marl source rocks is shown in Figure 12. Again, the NSO and asphaltene fractions plot similarly as with the siliciclastic group.

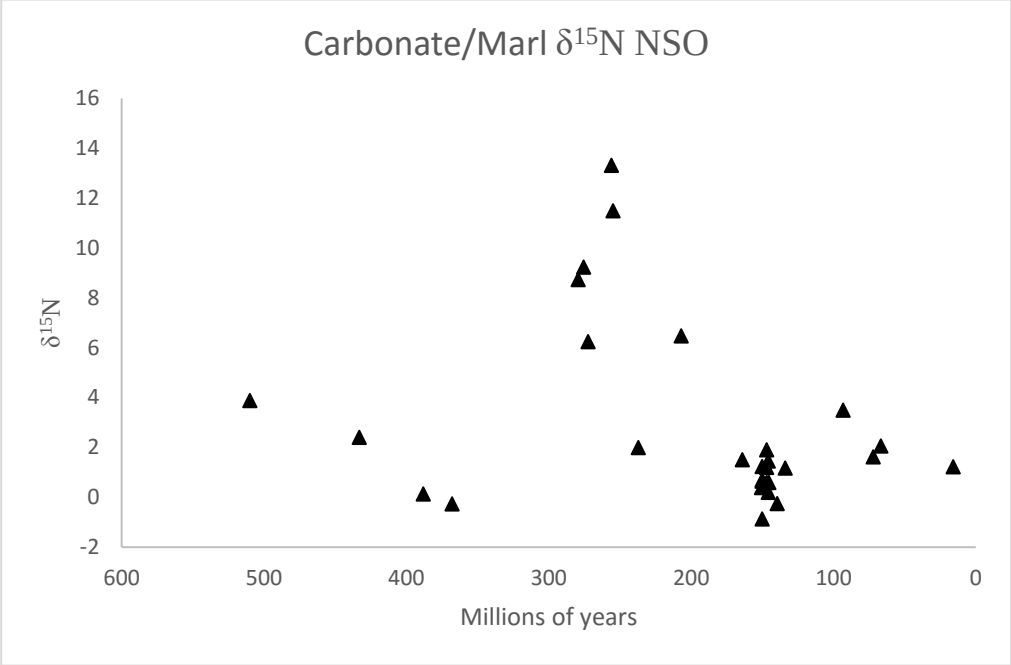

Figure 11. Oils derived from Carbonate/Marl source rocks of the sixty-two crude oils NSO values plotted against each oil's geologic age.

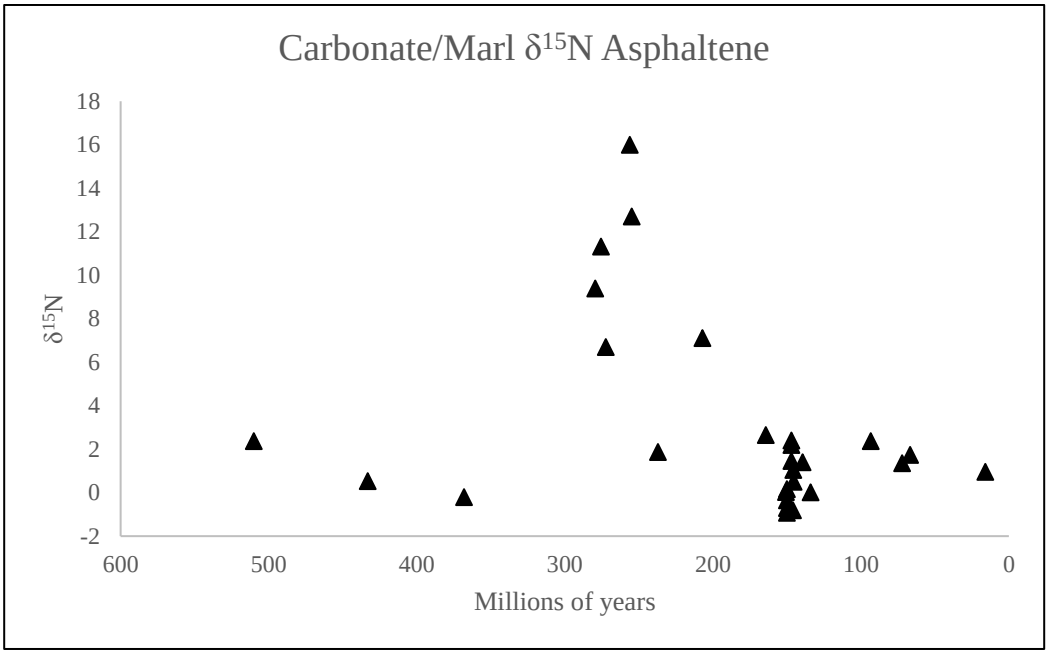

Figure 12. Oils derived from Carbonate/Marl source rocks of the sixty-two crude oils asphaltene values plotted against each oil's geologic age.

The combined NSO and asphaltene $\delta^{15}N$ values of oils derived from the two hypersaline and one lacustrine source rocks is shown in Figure 13. Sample 40 is from a lacustrine deposit and shows a small variation between the NSO and asphaltene fractions with an NSO value of 5.04‰ and asphaltene value of 3.20‰. However, sample 47 shows the greatest variability in all sixty-two samples between the NSO fraction and the asphaltene fraction with a difference of 3.25‰.

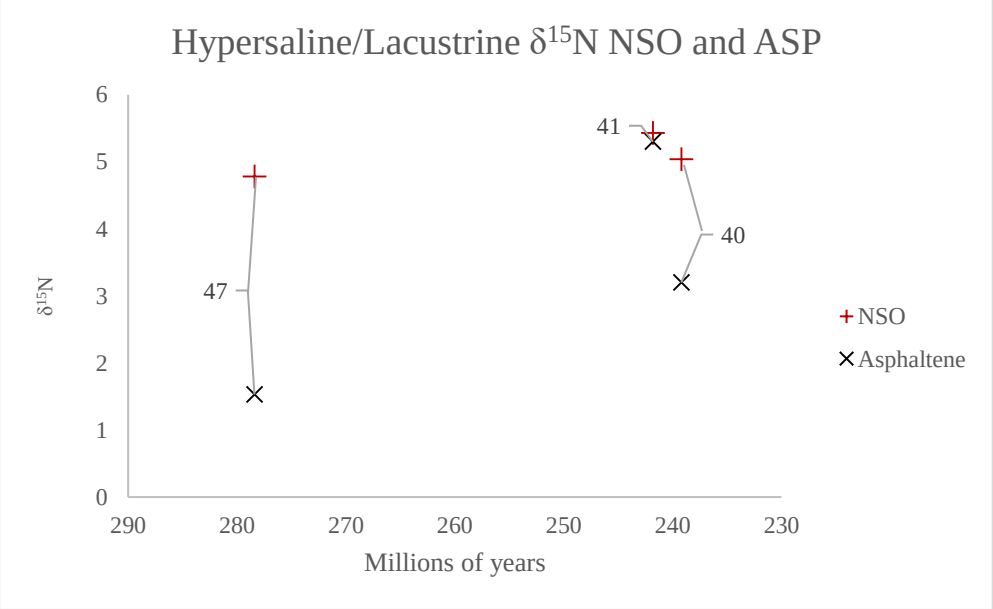

Figure 13. Oils derived from hypersaline/lacustrine source rocks of the sixty-two crude oils NSO and asphaltene values plotted against each oil's geologic age. Each point is labeled with corresponding ID from Appendix 1.

The combined NSO $\delta^{15}N$ values for all sixty-two crude oils is shown in Figure 14. The combined asphaltene $\delta^{15}N$ values for all sixty-two crude oils is shown in Figure 15. Both the NSO and asphaltene fractions show similar $\delta^{15}N$ values for geologic ages. The $\delta^{15}N$ values appear to be independent of source rock type.

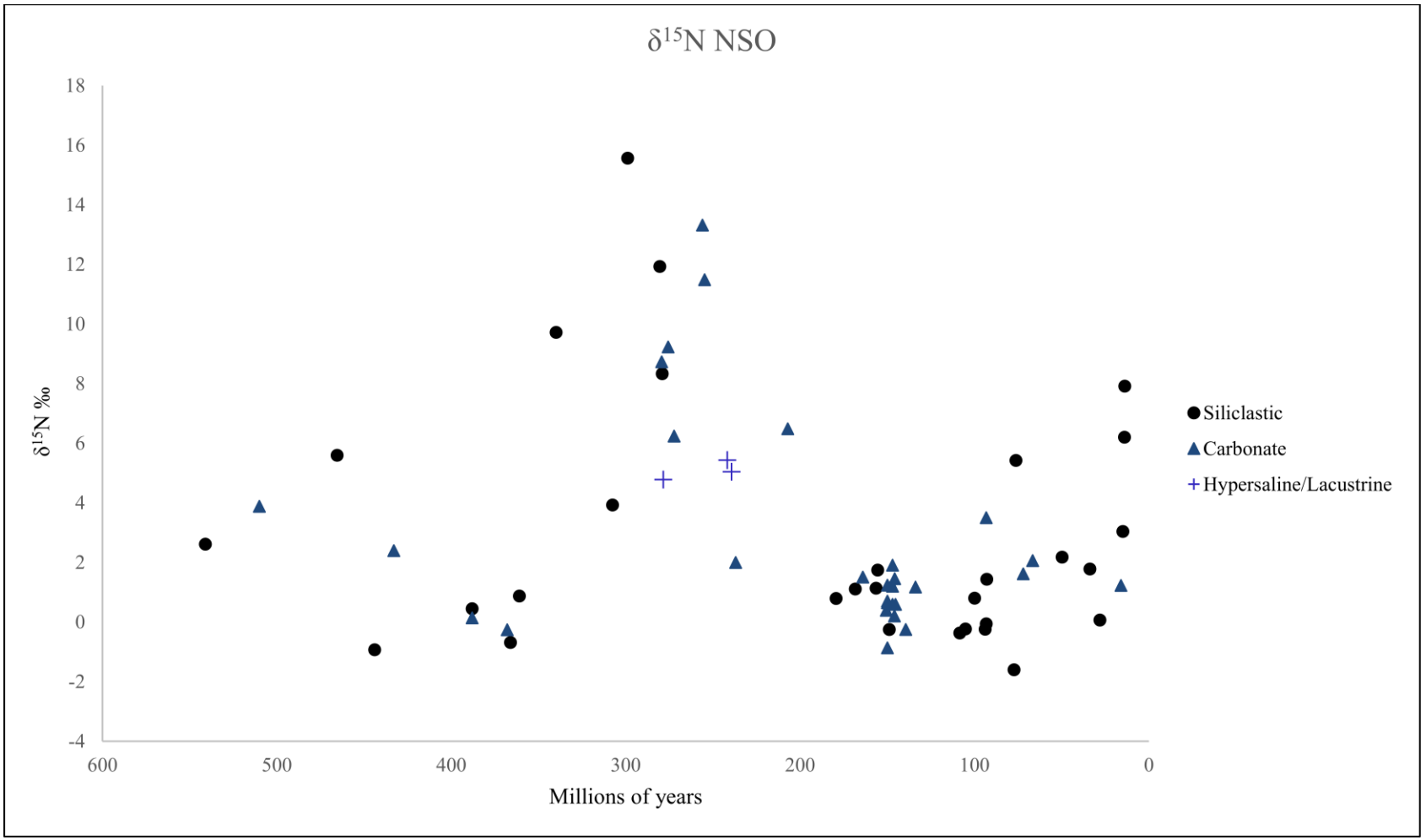

Figure 14. The combined NSO values for all depositional environments for each oil plotted against each oil's respective geologic

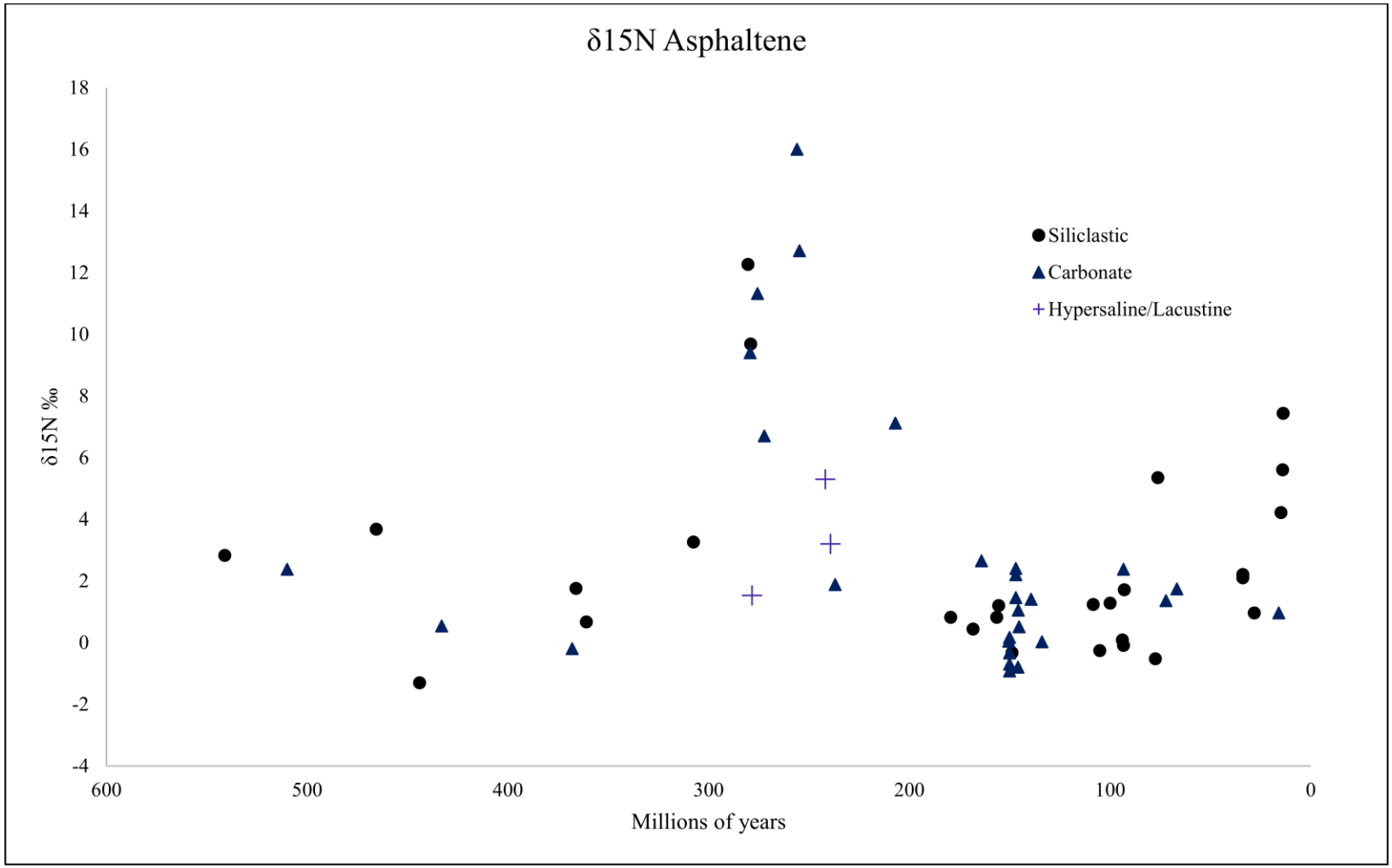

Figure 15. The combined asphaltene values for all depositional environments for each oil plotted against each oil's respective geologic age.

The combined NSO and asphaltene fractions for all sixty-two crude oils are shown in Figure 16. The siliciclastic and carbonate/marls ranging in age from the Cambrian to Ordovician become enriched in ^{15}N for both the NSO and asphaltene fractions, with values increasing from 2.38‰ to 5.60‰. The Silurian to Devonian age oils were depleted in ^{15}N relative to the Cambrian to Ordovician time range, with siliciclastic and carbonate/marl NSO and asphaltene values ranging from -1.30‰ to 2.40‰. Siliciclastic, carbonate/marl, hypersaline and lacustrine environments all exhibit a secular enrichment of ^{15}N for both the NSO and asphaltene fractions from the Upper Mississippian to the Triassic, with values ranging from 1.53‰ to 16.00‰.

The Lower Jurassic to the Paleogene has a similar trend to that of the Silurian to Devonian time span and is depleted in ^{15}N relative to the Upper Mississippian to the Triassic. Siliciclastic and carbonate/marls for both the NSO and asphaltene fractions range from -1.60 to 2.65‰. There are two exceptions in samples 11 and 13, which are enriched in ^{15}N. Sample 11 has an NSO value of 5.42‰, and asphaltene value of 5.35‰. Sample 13 has an NSO value of 3.50‰ and an asphaltene value of 2.38‰. The siliciclastic samples in the Neogene age are enriched in ^{15}N for both the NSO and asphaltene fractions, with values ranging from 3.04‰ to 7.92‰. Sample 3 from the Neogene age is derived from a carbonate source rock and is depleted in ^{15}N compared to the siliciclastic derived oils, with an NSO value of 1.23‰ and an asphaltene value of 0.96‰.

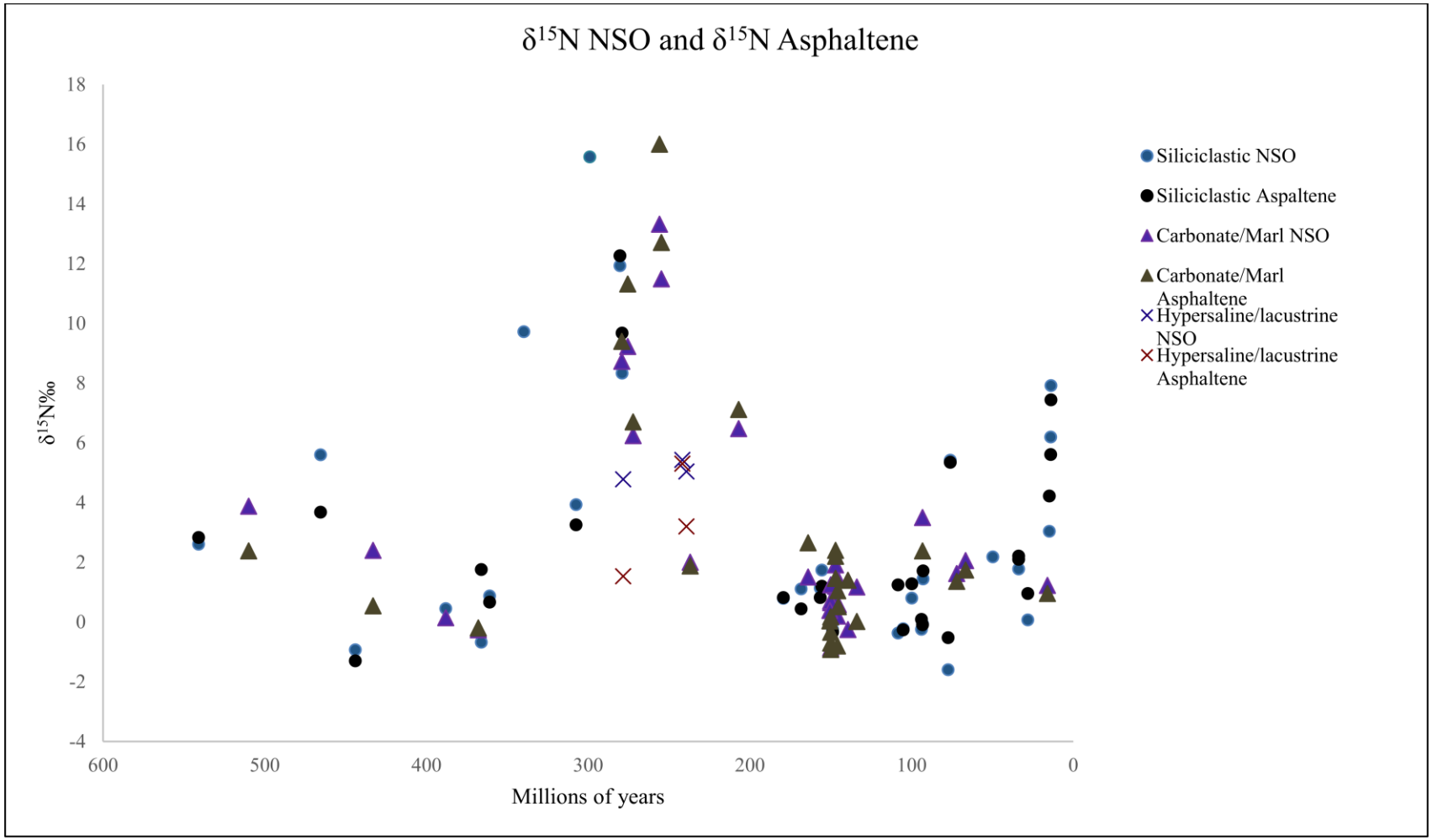

Figure 16. The combined NSO and asphaltene values for all depositional environments for each oil plotted against each oil's respective geologic age.

Discussion

Discussion of the $\delta^{15}N$ values with increasing thermal maturity of the Mexican oils

The use of nitrogen isotopes as a redox proxy or to reconstruct paleo environments relies on the preservation of the primary isotope signal. It is, therefore, necessary to determine if and to what extent the nitrogen signal is affected by diagenesis and catagenesis, which can lead to the alteration of the primary isotope signal (Williams et al., 1995; Lehmann et al., 2002; Knies et al., 2007; Robinson et al., 2012; Quan et al., 2013; and Rivera et al., 2015).

The preservation of the primary nitrogen isotope signal depends on the condition in which organic matter is preserved (Quan et al., 2013). The preservation of organic matter depends on oxygen exposure time, as anoxic conditions enhance preservation, the rate of supply of organic matter to the sea floor, i.e. size of the particle and depth of the water column, bulk sedimentation rate, and the sealing efficiency which is driven by the sedimentation rates (Calvert et al., 1996; Lehmann et al., 2002; Oldenburg et al., 2007; Möbius et al., 2011; Rivera et al., 2015). Preservation is, therefore, greater in oxygen minimum zones and in areas of high sedimentation where sediment sealing efficiency is large. The opposite is therefore true and preservation is low in high oxygen concentrations where the rate supply of organic matter is low.

In organic preserving environments, there appears to be little to no alteration of the initial $\delta^{15}N$ values (Macko and Quick and references therein, 1986; Quan et al., 2013; Rivera et al., 2015), while low organic preserving environments in both down core profiles, geologic records, and incubation experiments show an increase in $\delta^{15}N$

(Möbius et al., 2011; Robinson et al., 2012). However, Robinson et al., (2012) show through empirical data that even in slowly accumulating regions found in the ocean, the bulk sedimentary $\delta^{15}N$ values reflect the $\delta^{15}N$ values of the sinking organic matter.

Apart from early and water column diagenesis, mechanisms for post-burial degradation of organic matter include sedimentary diagenesis and thermal maturity. Terrestrial input can affect the primary nitrogen isotope signal. Diagenesis results in the biological and thermal degradation of organic matter which produces NH_4. This ammonium can then be incorporated in clay layers and feldspars. Because these minerals were altered by the decomposition of the organic matter, they share a very similar isotopic signal to the organic matter from which it was formed, resulting in little net isotope effect (Rau et al., 1987; Oldenburg et al., 2007; Schimmelmann and Lis, 2010; Robinson et al., 2012). Thermal alteration in organic matter causes the preferential release of ^{14}N as it takes less energy to break than that of a bond of ^{15}N-^{12}C, therefore enriching the kerogen in ^{15}N relative to the crude oil (Rau et al., 1987; Williams et al., 1995). However, both Boudou et al., (2008) and Vandenbroucke and Largeau (2007) found that only at the end of the oil and natural gas window will nitrogen be released from kerogen as N_2, and there is no systematic enrichment in $\delta^{15}N$ in samples of increasing maturity.

Lastly, biodegradation of oils preferentially removes the ^{14}N as biochemical reactions take place. This leaves the remaining substrate of oil enriched in ^{15}N (Kern et al., 2016). With increasing biodegradation, the remaining oil substrate becomes increasingly enriched in ^{15}N (Chuanping, et al., 2005). Marcano et al. (2013), however, did not observe any systematic isotopic change in bulk bitumen with increasing

biodegradation. However, they did acknowledge specific compounds including carbazole, alkylcarbazoles and benzo[b]carbazoles in the NSO and asphaltene fractions of oil change in both concentration and distribution with biodegradation.

If initial $\delta^{15}N$ values are affected by thermal maturity, then the NSO and asphaltene fractions in crude oils should exhibit isotopic enrichment from immature to mature oil as characterized by their API gravity and Ts/Tm values. In the Mexican oils, sample 22 is enriched in ^{15}N relative to sample 33 despite sample 22 having a low API gravity. However, when looking at the C_{27} Ts/Tm and C_{29} Ts/Tm parameters, sample 22 has a higher maturity than that of sample 33. This can be explained by sample 22 being heavily biodegraded as shown in the whole crude oil gas chromatogram (Figure 17). Sample 22 is from the Tampico basin, while the other four Mexican oils are from the Sureste basin and show no evidence of biodegradation (Figures 18 to 21).

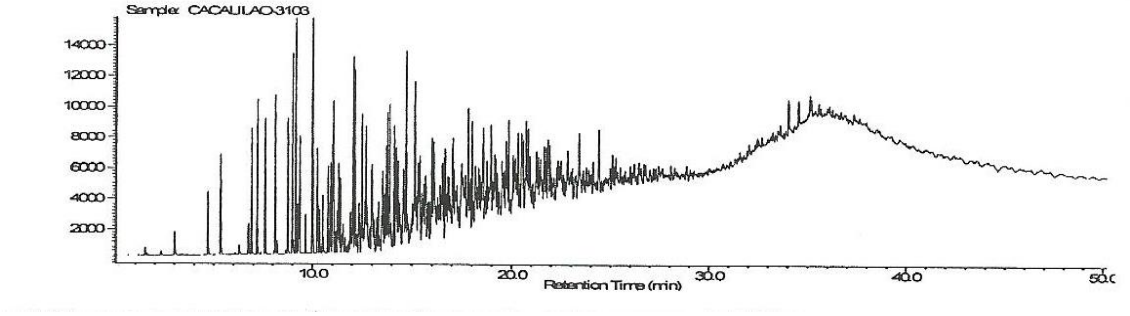

Figure 17. Chromatogram of sample 22 of the Tampico basin showing heavy biodegradation (courtesy of GeoMark Research, Houston, TX).

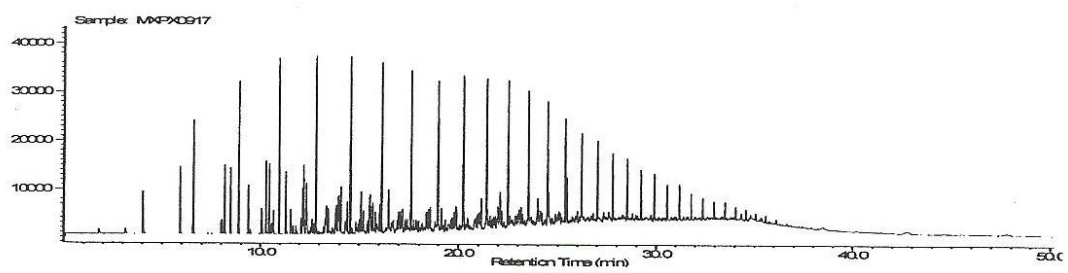

Figure 18. Chromatogram of sample 33 of the Sureste basin (courtesy of GeoMark Research, Houston, TX).

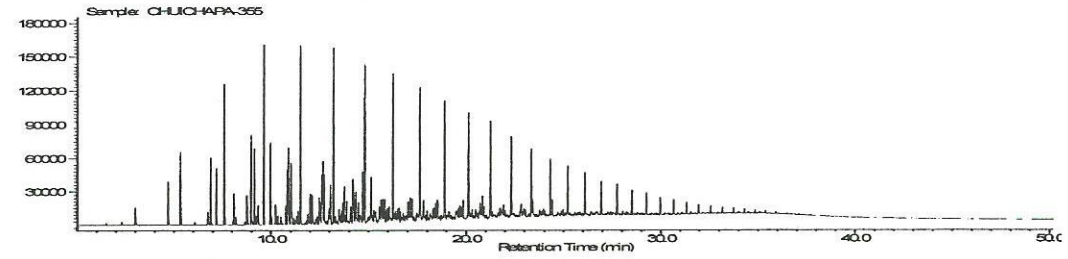

Figure 19. Chromatogram of sample 31 of the Sureste basin (courtesy of GeoMark Research, Houston, TX).

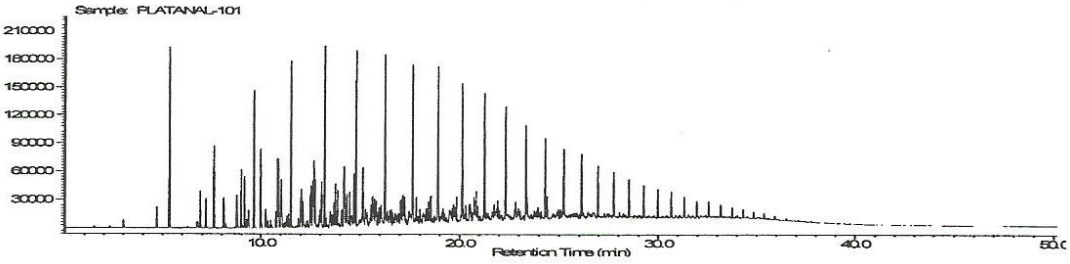

Figure 20. Chromatogram of sample 32 of the Sureste basin (courtesy of GeoMark Research, Houston, TX).

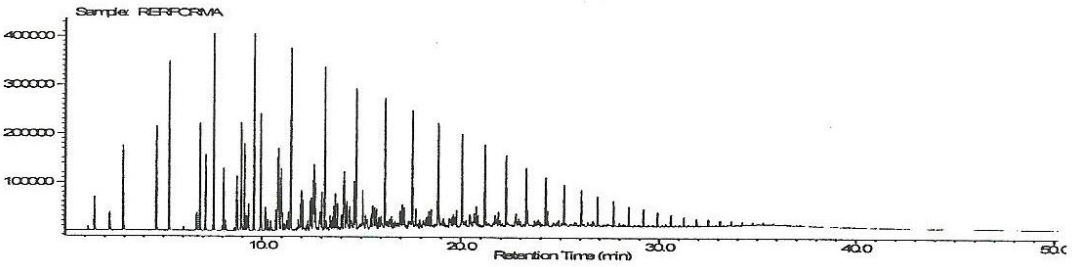

Figure 21. Chromatogram of sample 30 of the Sureste basin (courtesy of GeoMark Research, Houston, TX).

Depositional environment plays an important role when determining thermal effects of the primary nitrogen isotope signal. As stated earlier, to evaluate the effects of thermal maturity, an assumption is made that the organic matter from which the oils were derived is deposited under the same conditions and depositional environments (Rivera, 2013). Sample 22 from the Tampico basin is heavily biodegraded, whilst the other Mexican oils from the Sureste basin are not. The presence of heavy biodegradation of one oil and the exclusion of biodegradation in the other oils, is evidence that sample 22 was not deposited under the same conditions as oils from the Sureste basin, or was subject to different alterations after deposition and therefore cannot be evaluated for thermal maturity relative to the oils from the Sureste basin.

The oils from the Sureste basin also show a change in depositional environment from anoxic conditions in the immature sample 33 to a more oxic environment in the mature sample 30. The concentration of sulfur is the highest in sample 22 at 4.12% and steady decreases until it reaches 1.23% in sample 30 (Table 5, data provided by GeoMark research, Houston, TX). High sulfur concentration can be an indication for anoxic conditions as well large vanadium and nickel V/V+Ni ratios (Peters et al., 2005; Galarraga et al., 2008). The V/V+Ni ratios start out high in sample 33, and as sulfur did, decreased steady until sample 30. Sample 33 also shows a lower pristane/phytane (Pr/Ph) ratio than that of the other 3 oils (Table 5). The enrichments in ^{15}N could therefore be an indication for a change in depositional environments rather than thermal enrichment.

Table 5.

Depositional environment parameters for the Mexican Oils. (courtesy of GeoMark research, Houston, TX)

Sample ID	%S	ppm V	ppm Ni	V/V+Ni	Pr/Ph
22	4.41	550	72	0.88	Not available
33	4.12	1520	84	0.95	74
31	3.19	114	17	0.87	1.05
32	1.67	41	10	0.80	1.02
30	1.23	23	22	0.51	1.01

The NSO fraction of the remaining Sureste basin oils show a slight enrichment in ^{15}N with increasing API gravity and slight increasing maturity. The asphaltene fraction of the remaining Sureste basin oils also show a slight enrichment in^{15}N in samples 33, 31, and 32. However, the asphaltene fraction of sample 30 is depleted in ^{15}N relative to sample 32 and 31 despite sample 30 being of the highest maturity whilst sample 30 shows the greatest variance between the NSO and asphaltene fractions with a difference of 0.54‰.

Each Mexican oil also shows an ^{15}N enrichment of the NSO fraction compared to that of the asphaltene fraction. It is widely accepted that the asphaltene fraction is the most resistant to biodegradation as well as other geological process including thermal maturity (Snowdon et al., 2016 and references therein). There is a relative increase in the concentration of the asphaltene and NSO fractions as less resistant compounds in the saturate and aromatic fractions are consumed, and as asphaltenes selectively remove nitrogen from kerogen (Macko and Quick and references therein, 1986; Liao et al., 2009; Rivera et al., 2015) Nitrogen compounds are altered through the selective loss of

the least condensed compound. The NSO fraction is distinguished by likely having the least condensed nitrogen compounds and asphaltenes the more condensed nitrogen compounds (Liao et al., 2009). This could mean that the NSO fraction is more susceptible to biodegradation and thermal maturity. Thermal maturity in organic matter will preferentially cleave the light isotope (^{14}N) leaving the substrate enriched in ^{15}N. This could account for the enrichment in ^{15}N in the NSO relative to the asphaltene fraction.

Discussion of the $\delta^{15}N$ values with increasing thermal maturity of the Middle Eastern oils

The Middle Eastern oils are enriched in ^{15}N with increasing maturity in samples 21, 27, and 26 in both the NSO and asphaltene fractions. However, sample 25 is depleted in ^{15}N compared to sample 26, in both the NSO and asphaltene fractions, despite sample 25 having the highest maturity and API gravity. There isn't a strong correlation in sulfur content, V/V+Ni ratios and Pr/Ph ratios with increasing maturity as was observed for the Mexican oils. The sulfur content is higher in the most immature sample 21 and decreases steadily with increasing maturity (Table 6, data provided by GeoMark research, Houston, TX). The V/V+Ni ratios also decrease with increasing maturity, but are almost the same in sample 26 and 25. Sample 25 has a lower Pr/Ph ratio than that of sample 27 and 26, but is very similar to that of sample 21 (Table 6). It is therefore unlikely that a change in depositional environment has taken place and does not account for the depletion in ^{15}N in sample 25 relative to 26.

Table 6.

Depositional environmental parameters for the Middle East Oils (courtesy of GeoMark research, Houston, TX)

Sample ID	%S	ppm V	ppm Ni	V/V+Ni	Pr/Ph
21	2.51	134	31	0.81	0.64
27	2.11	35	7	0.83	0.74
26	2.19	27	13	0.68	0.79
25	1.58	23	12	0.66	0.66

The Middle Eastern oils are also unlike the Mexican oils in that their asphaltene fractions are enriched in ^{15}N compared to the NSO fractions for each oil. As stated above, the asphaltene fraction is more resilient and less likely to be altered by thermal alteration. Macko and Quick, (1986) suggest that the asphaltene selectively removes nitrogen from the kerogen. Because the NSO fraction is more susceptible to thermal alteration, the concentration of nitrogen could be more depleted than in the asphaltene fraction, accounting for the enrichment of ^{15}N in the asphaltene relative to the NSO fraction.

Discussion of the $\delta^{15}N$ values for the sixty-two crude oils over geologic time.

As stated above, the signal of nitrogen isotopes in sedimentary organic matter can improve our understanding of the past nitrogen cycle (Godfrey & Glass, 2011; Tesdal et al., 2013; Saitoh et al., 2014) and be used to determine past biochemical cycling in the paleo-oceanographic record. However, the use of the nitrogen isotopic signal to reconstruct paleo-environments relies on the preservation of the primary nitrogen isotopic signal (Godfrey & Glass, 2011; Quan et al., 2013). The thermal maturity study discussed above does not show a systematic enrichment in ^{15}N with increased maturity. Also, Tesdal et al. (2013) found that diagenetic alterations did not eliminate the preservation of nitrogen isotope fractionation variability. Diagenetic overprinting would result in a small standard deviation in $\delta^{15}N$ values throughout geologic time, which isn't observed in Tesdal's et al. (2013) data or found in this study. Therefore, the primary signal is likely preserved and can be used to understand the nitrogen cycle throughout geologic time.

The $\delta^{15}N$ values of crude oils derived from source rocks of known geologic age compared to the bulk $\delta^{15}N$ values previously reported for kerogens and sediments of similar geologic age (Algeo et al., 2012; Schoepfer et al., 2012; Knies et al., 2013; Saitoh et al., 2014; Grasby et al., 2015; and Stüeken et al., 2015 and references therein) is shown in Figure 23. The literature curve was constructed by taking an average of $\delta^{15}N$ values for samples from each unmetamorphosed basin and formation in the above-mentioned literature. The data sets match up well and show similar enrichments and depletions in ^{15}N with geologic time. The data sets and trends from the literature also appear to be independent of source rock type.

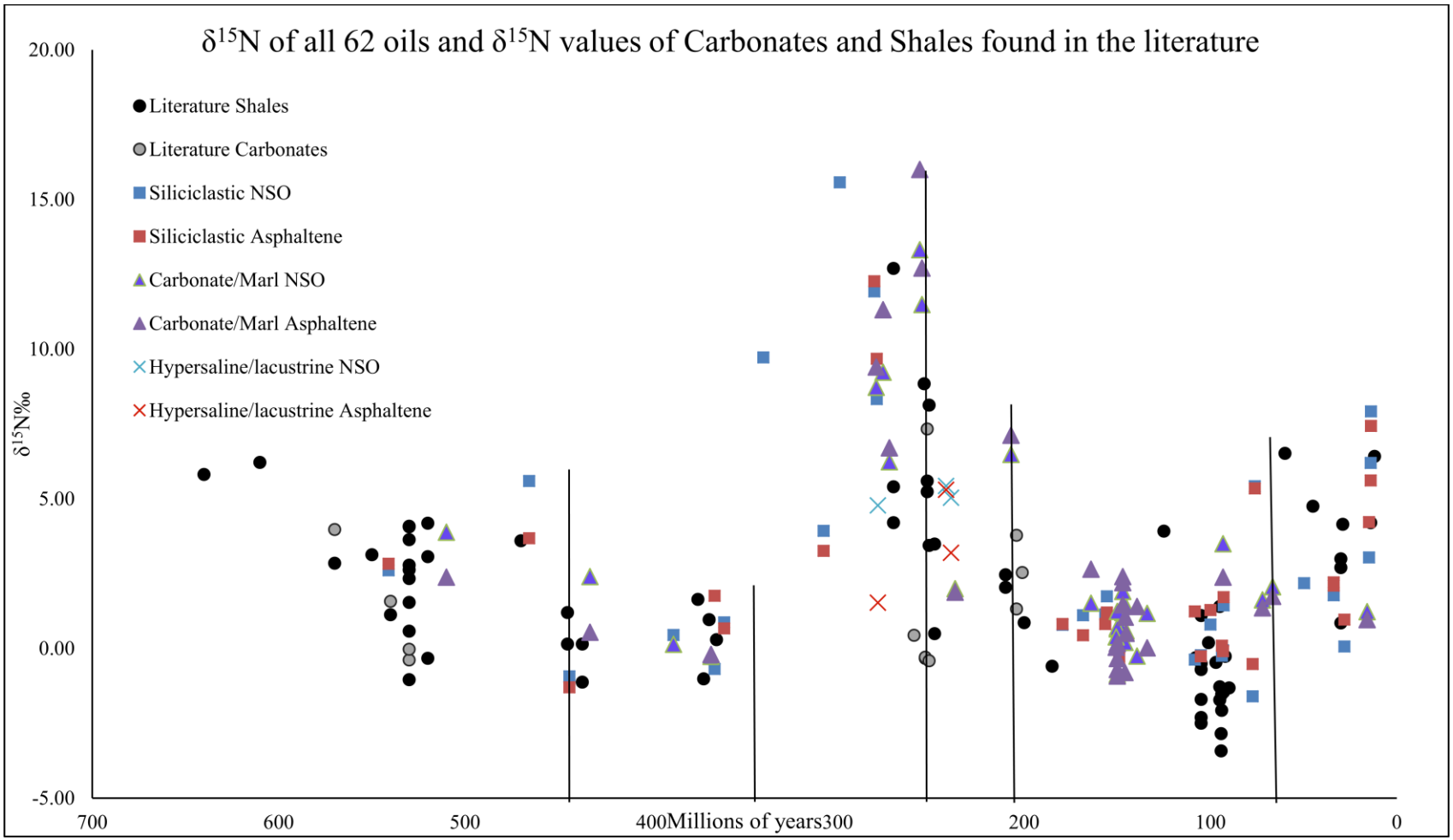

Figure 22. The sixty-two-crude oil NSO and asphaltene values compared to ^{15}N values of shales and carbonates found in published literature: Algeo et al., 2012; Schoepfer et al., 2012; Knies et al., 2013; Saitoh et al., 2014; Grasby et al., 2015; and Stüeken et al., 2015 and references therein. Vertical lines represent mass extinction events at the Late Ordovician, Late Devonian, Late Permian, Late Triassic, and the Late Cretaceous, respectively.

The oldest samples measured are from the Precambrian/Cambrian. Samples from siliciclastic and carbonate/marl plot similarly for both the NSO and asphaltene from the Precambrian/Cambrian to the Ordovician. The $\delta^{15}N$ values range from 2.38 to 5.60‰. However, the bulk kerogen data from the literature have older Precambrian $\delta^{15}N$ values that are enriched in ^{15}N relative to the Cambrian to Ordovician $\delta^{15}N$ values. The depletion in ^{15}N of the Cambrian samples is thought to reflect the onset of the Cambrian "explosion" (Kikumoto et al., 2014; Wang et al., 2015). New life, including multicellular animals lead to a more biologically controlled geological record and more sophisticated feedback systems (Ader et al., 2014; Cremonese et al., 2013; Cremonese et al., 2014). A shift to more oxic waters from anoxic waters in the Precambrian would shift nitrate limited waters to nitrate enriched waters (Kikumoto et al., 2014). When assimilation of nitrate takes place, the light isotope is preferentially taken up into organic matter, making the organic matter depleted in ^{15}N, thus decreasing the $\delta^{15}N$ values (Kikumoto et al., 2014).

Next, the Silurian to Devonian age samples are depleted in ^{15}N relative to the Cambrian to Ordovician $\delta^{15}N$ values. Siliciclastic and carbonate/marl NSO and asphaltene values range from -1.30‰ to 2.40‰. These values are more consistent with $\delta^{15}N$ of atmospheric N_2, except the more enriched asphaltene fraction in sample 54, with a $\delta^{15}N$ value of 1.76‰, and the more enriched NSO fraction in sample 59, with $\delta^{15}N$ value of 2.40‰. This would suggest that nitrogen fixation was the main source of biologically available nitrogen as nitrogen fixation isotope fractionation is small which result in $\delta^{15}N$ values of -2 to 0‰ (Meckler et al., 2011; Kilumoto et al., 2014; Luo et al., 2016).

A shift from nitrification and assimilation in oxic waters during the Cambrian and the Ordovician to nitrogen fixation in anoxic waters during the Silurian through the Devonian is thought to have occurred when the Late Ordovician underwent mass extinctions (Zhang et al., 2009) due to severe climate change causing significant fluctuations in the marine environment (Melchin et al., 2013; Zhou et al., 2015; Luo et al., 2016). Global cooling lead to a short glacial period during the Late Ordovician (Sheehan, 2001; Melchin et al., 2013; Zhou et al., 2015). After glaciation, an onset of rapid global warming resulted in a rapid sea level rise, decreased ocean circulation and intensified the oceanic chemocline contributing to the growth of anoxia in ocean waters (Melchin et al., 2013; Zhou et al., 2015). In stratified anoxic marine environments, nitrogen fixation is the dominant process where biologically available fixed nitrogen is scarce due to the significant loss of fixed nitrogen through the denitrification and anammox processes (Luo et al., 2016 and references therein). Low $\delta^{15}N$ values could therefore reflect the development of extensive oceanic anoxia during the post-glacial eustatic sea level rise in the Late Ordovician.

The Devonian age is also characteristic of anoxic waters (Calvert et al., 1996) and reduced surface- water productivity (Levman and von Bitter, 2002) as observed by low $\delta^{15}N$ values. Again, there was a mass extinction in the Late Devonian (Bingham-Koslowski et al., 2016) thought to have been caused by the extensive anoxia in the water column (Liu et al., 2016 and references therein). As described above, nitrogen fixation is the dominant process in anoxic waters and reflect $\delta^{15}N$ values of -2‰ to 0‰ (Strąpoć et al., 2010; Meckler et al., 2011; Kilumoto et al., 2014; Luo et al., 2016). Intensification of the marine anoxic water column is generally associated with global

warming and a more intense oceanic stratification. A compilation of $\delta^{15}N$ values for marine sediments indicated that greenhouse climates are characterized by low $\delta^{15}N$ values ranging from -2‰ to 2‰ (Algeo et al., 2014). These values fit the values seen in the Devonian of the present study very well.

Entering the Upper Mississippian, the samples are enriched in ^{15}N relative to the Silurian and Devonian times. The samples are progressively enriched in ^{15}N with decreasing age until the Late Permian. The $\delta^{15}N$ values for this time interval range from 1.53‰ to 16.00‰ (Figure 23). Algeo et al. (2008) also observed high $\delta^{15}N$ values for bulk sediment (10‰ to 14‰) in the Upper Carboniferous. The nitrogen values indicate a trend towards global cooling and continental glaciation (Liu et al., 2016). This is also supported by well-preserved oxygen isotopes that show an enrichment in ^{18}O for brachiopod calcite, and conodont apatite, reflecting temperature and ice volume effects (Saltzman, 2002 and references therein; Wallace and Elrick, 2014). An explanation for the enrichment in ^{15}N could be eustatic sea level fall related to increased continental ice mass. This would cause a reduction in the amount of denitrification present in the shelf sediments, and shift the denitrification process into continental slope oxygen minimum zones leading to higher fractionation effects (Liu et al., 2016). Also, global changes in ocean circulation patterns could have led to strengthened cold-water upwelling on continental margins, creating an expanse of the oxygen-minimum zones. Anoxic waters from the Devonian period would start to subside, which would then lead to an increase in water column denitrification and higher $\delta^{15}N$ values (Algeo et al., 2008 and references therein; Schoepfer et al., 2012; Grasby et al., 2016; Liu et al., 2016). A compilation of $\delta^{15}N$ values for marine sediments indicated that icehouse climates are

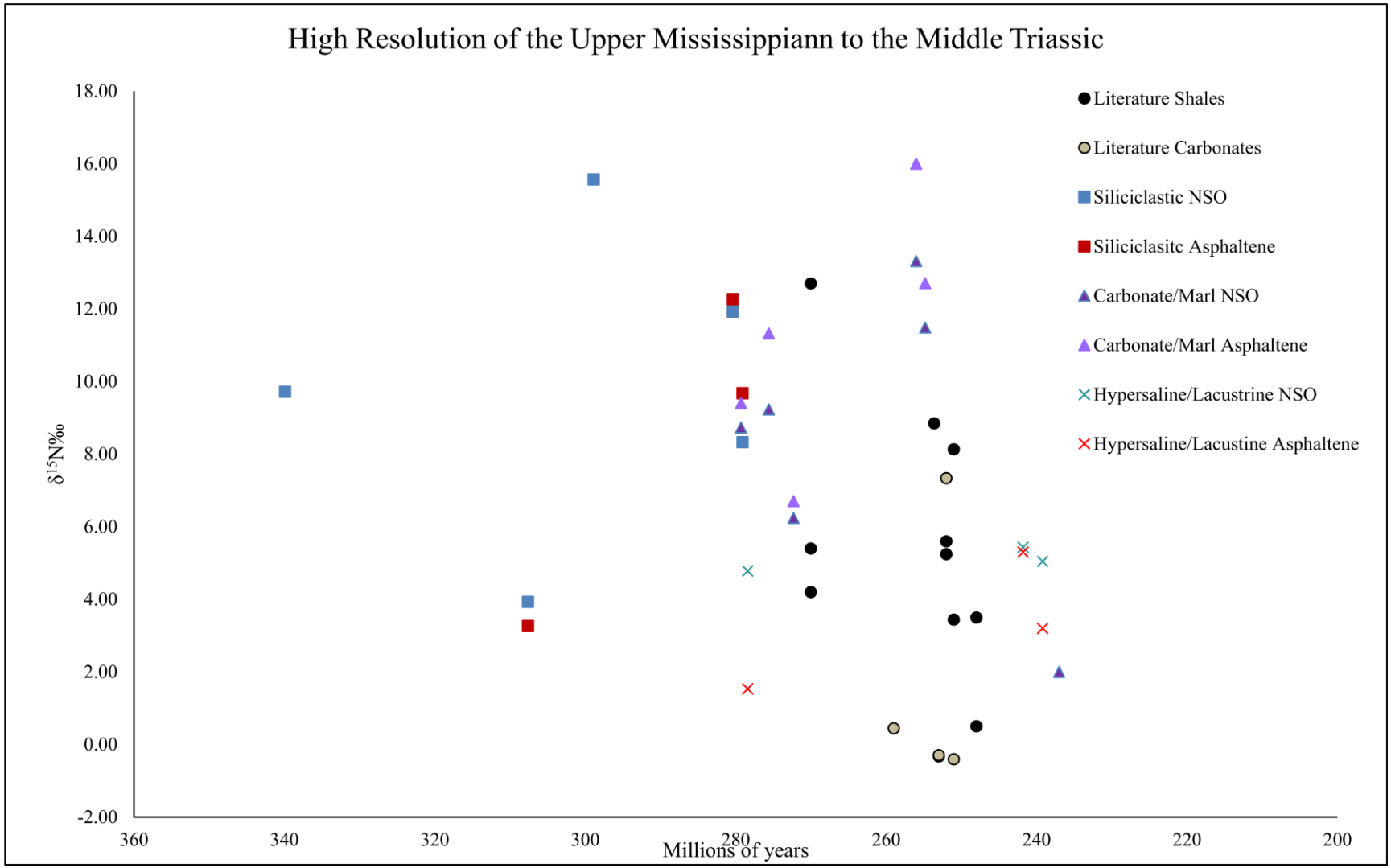

Figure 23. The Upper Mississippian to the Middle Triassic oils of both NSO and asphaltene fractions in high resolution.

characterized by high $\delta^{15}N$ values ranging from 4‰ to 8‰ (Algeo et al., 2014). The high variation observed in the $\delta^{15}N$ values during the Upper Mississippian to the Permian (Figure 23) could have been caused by the growth and decline of the continental ice mass, which caused global sea level to vary. The $\delta^{15}N$ values are thought to peak in concurrence with deglacial transgression, and gradually return to normal sea values (4‰ to 8‰) before fully interglacial conditions are reached (Algeo et al., 2008).

After the Late Permian, a progressive decrease in the δ15N values continues until the Neogene. The Late Permian extinction could have caused the fall in $\delta^{15}N$ values in the Triassic period. The Late Permian extinction is characterized by being the worst mass extinction in Earth history (Schoepfer et al., 2012; Grasby et al., 2015; Grasby et al., 2016) which eliminated 90% of marine species and 70% of terrestrial species (Luo et al., 2011; Grasby et al., 2015). The cause of the extinction is thought to have occurred with the eruption of the Siberian Traps (Schoepfer et al., 2012; Sun et al., 2012; Saitoh et al., 2014; Grasby et al., 2015), which caused global warming due to the expulsion of CO_2 into the air. Well-preserved oxygen isotopes in conodont apatite show depleted ^{18}O, supporting rapid warming and extremely high oceanic temperatures during this mass extinction (Sun et al., 2012). Acidic ocean conditions could therefore have developed, and global anoxia has been well established for this time (Luo et al., 2011; Schoepfer et al., 2012; Grasby et al., 2015). Upwelling along the northwest margin of Pangea would have stopped due to increased sea-surface temperature (Sun et al., 2012; Grasby et al., 2016) further stratifying the water column. Decreased upwelling coupled with anoxic waters would lead to nitrate limited waters and enhanced nitrogen

fixation (Luo et al., 2011; Schoepfer et al., 2012; Knies et al., 2013; Grasby et al., 2016).

After the progressive depletion of $\delta^{15}N$ values in the Triassic, $\delta^{15}N$ values remain fairly consistent in the Jurassic up until the Paleogene. The $\delta^{15}N$ values range from -1.60‰ to 2.65‰. Samples 11 and 13 are enriched in ^{15}N compared to the other samples in the Late Cretaceous. The boundary between the Late Triassic and Early Jurassic is marked by yet another extinction event which is then followed by the Toarcian Oceanic Anoxic Event (Jenkyns et al., 2001 and references therein; Fujisaki et al., 2016; Schoepfer et al., 2016). Again, the Jurassic is characterized by widespread anoxia and euxinic water column conditions by the Late Jurassic (Fujisaki et al., 2016; Schoepfer et al., 2016). The nitrate supply would again be limited, making nitrogen fixation the primary process with a fractionation close to the $\delta^{15}N$ value for atmospheric N_2.

The Cenomanian and Turonian boundary is also characterized by an Oceanic Anoxic Event (Junium and Arthur, 2007; Núñez-Useche et al., 2016 and references therein). As with the Jurassic, this lead to widespread anoxia and euxinic waters as seen in the Jurassic. The primary process is, therefore, nitrogen fixation (Rau et al., 1987; Kuypers et al., 2004; Junium and Arthur, 2007; Algeo et al., 2008). Sample 13 is enriched in ^{15}N compared to the other values at the Cenomanian-Turonian time. However, the asphaltene value (2.38‰) in sample 13 is only slightly enriched from $\delta^{15}N$ values seen for greenhouse climates ranging from -2‰ to 2‰ (Algeo et al., 2014). The enrichment of the NSO fraction relative to the asphaltene fraction for sample 13 could be due to diagenesis. Sample 11 is enriched in ^{15}N for both the NSO and

asphaltene fractions compared to other samples of the Late Cretaceous. This is perhaps an isolated signal to this specific location (Sirte Basin, Libya) where denitrification is more abundant due to reduced anoxia in the area or better water circulation and upwelling. Another possibility could include more terrestrial organic matter input. Rau et al. (1987) found that $\delta^{15}N$ values were higher for Cretaceous samples containing more terrigenous organic matter input. More research at this particular sight would need to be performed to further understand the nitrogen cycle, the organic source material, and redox potentials which lead to an enrichment in ^{15}N.

The transition from the Cretaceous to the Paleogene was marked by another mass extinction thought to have been caused by an impact from an asteroid or other extraterrestrial body (Glasby and Kunzendorf, 1996 and references therein; Sepúleda et al., 2009 and references therein; Beckwith, 2013 and references therein; Mizukami et al., 2013 and references therein). The $\delta^{15}N$ values for this time are low and are similar to $\delta^{15}N$ values from the Jurassic and the Cretaceous. The impact of the asteroid would have caused atmospheric dust and sulfate aerosols leading to global cooling and darkening of the planet (Sepúleda et al., 2009 and references therein; Mizukami et al., 2013 and references therein) Many models are proposed for the oceanic chemistry that followed afterwards; including a large depletion in primary productivity, limiting the rate of supply of organic matter to the sea floor (Sepúleda et al., 2009 and references therein; Beckwith, 2013 and references therein). Darkening of the skies would have inhibited photosynthesis causing the extinction of many marine animals (Glasby and Kunzendorf, 1996; Sepúleda et al., 2009 and references therein; Mizukami et al., 2013 and references therein).

Low oxygen conditions in the oceans are characteristic in low to mid latitudes during the Cretaceous/Paleogene boundary with anoxic bottom waters and euxinia reported in some areas (Sepúleda et al., 2009; Mizukami et al., 2013 and references therein). High latitudes show less anoxia and Beckwith (2013), report $\delta^{15}N$ values that are higher than those from low to mid latitudes. Cyanobacteria were less affected by the extinction (Sepúleda et al., 2009), so nitrogen fixation could still take place. This is thought to be the primary control over the $\delta^{15}N$ values for this time, not because of an increase in nitrogen fixation but because of the decrease of eukaryotic productivity and nitrogen assimilation (Brisman et al., 2001; Sepúleda et al., 2009)

The $\delta^{15}N$ values become enriched in the Miocene. However, only the oils derived from siliciclastic source rocks show an enrichment. The one carbonate/marl sample does not show an enrichment in ^{15}N. The beginning of the Miocene is characterized by warm waters but a sudden shift towards glaciation and global cooling is seen around 14.7 to 13.9 million years (Holbourn et al., 2007; Verducci et al., 2009 and references therein; Majewski and Bohaty, 2010 and references therein). Global cooling and the advancement of ice sheets cooled sea surface temperatures and increased circulation. (Holbourn et al., 2007; Verducci et al., 2009 and references therein; Majewski and Bohaty, 2010 and references therein). Macko et al. (1990), also reported an enrichment of $\delta^{15}N$ values from the middle Miocene. They suggested that the enrichment was because of recycling of organic matter. The shift from greenhouse to icehouse conditions in the Middle Miocene would enrich $\delta^{15}N$ values to 4‰ to 8‰ (Algeo et al., 2014). Values in the Middle Miocene for this study range from 3.04‰ to 7.92‰ and correlate well to icehouse values. Increased nitrate supply would enable

denitrification to preferentially select the light isotope (^{14}N) thus enriching the remaining substrate. Increased circulation in the ocean leading to upwelling and recycling of nitrate in organic matter would therefore be enriched in ^{15}N.

A possible explanation for the carbonate/marl that doesn't show the enrichment in the Neogene could be because the carbonate/marl is slightly older than the siliciclastic samples from this time, reflecting the warmer global climate, thus having $\delta^{15}N$ values (NSO value of 1.23‰ and an asphaltene value of 0.96‰) that correspond to greenhouse $\delta^{15}N$ values (Algeo et al., 2014). Another explanation could be that the carbonate/marl was deposited in low latitudes (Palawan Shelf, Philippines) while the siliciclastic samples from the Miocene were deposited in high latitudes (San Joaquin Basin, United States). With increasing latitude, there is a decrease in $[NO_3^-]$ from increased production and assimilation. Therefore, the $\delta^{15}N$ values are higher in higher latitudes and the $\delta^{15}N$ values are lower in lower latitudes (Altabet and Francois, 1994; Saitoh et al., 2014).

Conclusions

The sixty-two crude oils derived from source rocks of known geologic age compared to the bulk $\delta^{15}N$ values previously reported for kerogens and sediments of similar geologic age (Algeo et al., 2012; Schoepfer et al., 2012; Knies et al., 2013; Saitoh et al., 2014; Grasby et al., 2015; and Stüeken et al., 2015 and references therein) appear to match up and show similar enrichments and depletions in ^{15}N with geologic time. Therefore, the nitrogen isotope composition of crude oils appears to reflect that of the kerogens from which they were derived.

Two enrichments in ^{15}N occur in the Carboniferous/Permian, and Miocene. The enrichment of the $\delta^{15}N$ values from the Carboniferous/Permian age and the Miocene age is thought to originate from icehouse global conditions. Circulation in the ocean waters increased leading to enhanced upwelling and recycling of organic matter. The nitrate supply would be abundant thus allowing denitrification to preferentially take up ^{14}N, enriching the remaining organic matter in ^{15}N.

Three depletions in ^{15}N occur in the Cambrian/Ordovician, Silurian/Devonian, and Triassic through the Paleogene. The depletions of the $\delta^{15}N$ values in the Cambrian/Ordovician (depleted compared to Precambrian values found in the literature Stüeken et al., 2015) is thought to originate from the Cambrian "explosion" characterized by new marine animals and oxic waters. This lead to depleted $\delta^{15}N$ values as the primary process for nitrogen in the ocean would be assimilation and nitrification.

The Silurian/Devonian age and the Triassic through the Paleogene depletion of the $\delta^{15}N$ values are thought to originate from greenhouse conditions coinciding with mass extinction events. Greenhouse conditions are characterized by a rise in sea level

and sea water temperatures, and decreased circulation in the ocean leading to anoxic and sometimes euxinic water conditions. Nitrate supply was scarce during global warming and the denitrification process would go to completion without isotope fractionation. This lead nitrogen fixation to be the primary process in the ocean resulting in low $\delta^{15}N$**.**

The depletion and enrichment of ^{15}N throughout the Phanerozoic appears to be independent of source rock type. For each geologic age, the $\delta^{15}N$ values of the oils are similar, irrespective of source rock type. The enrichments and depletion in ^{15}N trends seen in this study, therefore, appear to be global rather than local signals.

References

Ader, M., Sansjofre, P., Halverson, G. P., Busigny, V., Trindade, R. I. F., Kunzmann, M., and Nogueira, A. C. R. (2014) Ocean redox structure across the Late Neoproterozoic Oxygenation Event: A nitrogen isotope perspective. Earth and Planetary Science Letters, Vol. 396, pp. 1-13.

Algeo, T., Rowe, H., Hower, J. C., Schwark, L., Herrmann, A., and Heckel, P. (2008) Changes in ocean denitrification during Late Carboniferous glacial-interglacial cycles. Nature Geoscience, Vol. 1, pp. 709-714.

Algeo, T., Henerson, C.M., Ellwood, B., Rowe, H., Elswick, E., Bates, S., Lyons, T., Hower, J.C., Smith, C., Maynard, B., Hays, L. E., Summons, R. E., Fulton, J., and Freeman, K.H. (2012) Evidence for a diachronous Late Permian marine crisis from the Canadian Arctic region. GSA Bulletin, Vol. 124, pp. 1424-1448.

Algeo, T. J., Meyers, P. A., Robinson, R. S., Rowe, H., and Jiang, G. Q. (2014) Icehouse-greenhouse variations in marine denitrification. Biosciences, Vol. 11, pp. 1273-1295.

Altabet, M. (2005) Isotopic tracers of the marine nitrogen cycle: Present and past. *In* "Marine Organic Matter: Biomarkers, Isotopes and DNA," (J. K. Volkman ed.) pp. 251-293. Springer, Berlin.

Altabet, M. A., and Francois, R. (1994) Sedimentary nitrogen isotopic ratio as a recorder for surface ocean nitrate utilization. *In* "Global Biochemical Cycles," Vol. 8, pp. 103-116.

Andrusevich, V.E., Engel, M.H., Zumberge, J.E., and Brothers, L.A. (1998) Secular, episodic changes in stable carbon isotope compositions of crude oils. Chemical Geology, Vol. 12, pp. 59-72.

Beckwith, B. A. (2013) The marine nitrogen cycle across the Cretaceous-Paleogene boundary at Maud Rise. MS Thesis, Texas Tech University, pp. 1-58.

Bingham-Koslowski, N., Tsujita, C., Jin, J., and Azmy, K. (2016) Widespread Late Devonian marine anoxia in eastern North America: a case study of the Kettle Point Formation black shale, southwestern Ontario. Canada Journal of Earth Science, Vol. 53, pp. 837-855.

Boudou, J-P. Schimmelmann, A., Ader, M., Mastalerz, M., Sebilo, M., and Gengembre, L. (2008) Organic nitrogen chemistry during low-grade metamorphism. Geochimica et Cosmochimica Acta, Vol. 72, pp. 1199-1221.

Brisman, K., Engel, M. H., and Macko, S. A. (2001) Distribution, stereochemistry, and stable isotope composition of amino acids in K/T boundary sediments. Precambrian Research, Vol. 106, pp. 59-77.

Brunner, B., Contreras, S., Lehmann, M.F., Matantseva, O., Rollog, M., Kalvelage, T., Klockgether, G., Lavik, G., Jetten, M.S.M., Kartal, B. and Kuypers, M.M.M. (2013) Nitrogen isotope effects induced by anammox bacteria. Proc. Natl. Acad. Sci. USA, Vol.110, No. 47, pp. 18994-18999.

Calvert, S. E., Bustin, R. M. and Ingall, E. D. (1996) Infulence of water column anoxia and sediment supply on the burial and preservation of organic carbon in marine shales. Geochimica et Cosmochimica Acta, Vol. 60, pp. 1577-1593.

Canfield, Donald E., Glazer, Alexander N., and Falkowski, Paul G. (2010) The evolution and future of Earth's nitrogen cycle. Science, Vol. 330, pp. 192-196.

Chuanping, C., Bowen, M., and Yacheng, C. (2005) Nitrogen isotopic geochemical characteristics of crude oils in serveral basins of China. Science in China Ser. D Earth Sciences, Vol. 48, pp. 1211-1219.

Coplen T.B. (2011) Guidelines and recommended terms for expression of stable-isotope-ratio and gas-ratio measurement results. Rapid Commun. Mass Spectrom. Vol. 25, pp. 2538-2560.

Cremonese, L., Shields-Zhou, G., Struck, U., Ling, H. Och, L., Chen, X., and Li, Da. (2013) Marine biochemical cycling during the early Cambrian constrained by nitrogen and organic carbon isotope study of the Xiaotan section, South China. Precambrian Research, Vol. 225, pp. 148-165.

Cremonese, L., Shields-Zhou, G., Struck, U., Ling, H. and Och, L. (2014) Nitrogen and organic carbon isotope stratigraphy of the Yangtze Platform during the Ediacaran-Cambrian transition in South China. Palaeogeography, Papeoclimatology, Palaeoecology, Vol. 398, pp. 165-186.

de la Rue, S. R., Rowe, H. D., and Rimmer, S. M. (2007) Palynological and bulk geochemical constraints on the paleoceanographic conditions across the Frasnian-Famennian boundary, New Albany Shale, Indiana. International Journal of Coal Geology, Vol. 71, pp. 72-84.

Devol, A. H. (2008) Denitrification including anammox. *In* "Nitrogen in the Marine Environment" (2nd edition) Chapter 6, pp. 263-301. Elsevier.

Engel, M.H. and Zumberge, J.E. (2007) Secular change in the stable sulfur isotope composition of crude oils relative to marine sulfates and sulfides. The 23rd International Meeting on Organic Geochemistry, Torquay, UK, Book of Abstracts pp. 523-524.

Francis, Christopher A., Roberts, Kathryn J., Beman, J. Michael., Santoro, Alyson E., and Oakley, Brian B. (2005) Ubiquity and diversity of ammonia-oxidizing archaea in water columns and sediments of the ocean. Proc. Natl. Acad. Sci. USA, Vol. 102, pp. 14683-14688.

Fujisaki, W., Sawaki, Y., Yamamoto, S., Sato, T., Nishizawa, M., Windley, B. F., and Maruyama, S. (2016) Tracking the redox history and nitrogen cycle in the pelagic Panthalassic deep ocean in the Middle Triassic to Early Jurassic: Insights from redox-sensitive elements and nitrogen isotopes. Palaeogeography, Palaeoclimatology, Palaeoecology, Vol. 449, pp. 397-420.

Galarraga, F., Retegui, K., Martïnez, A., Martìnez, M., Llamas, J. F., and Márquez, G. (2008) V/Ni ratio as a parameter in palaeoenvironment characterization of nonmature medium-crude oils from several Latin American basins. Journal of Petroleum Science and Engineering, Vol. 61, pp. 9-14.

Galbraith, E.D., Kienast, M. and the NICOPP Working Group (2013) The acceleration of oceanic denitrification during glacial warming. Nature Geoscience Vol. 6, pp. 579-584.

Glasby, G. P., and Kunzendorf, H. (1996) Multiple factors in the origin of the Cretaceous/Tertiary boundary: the role of environmental stress and Deccan Trap volcanism. Geologische Rundschau, Vol. 85, pp. 191-210.

Godfrey, L. V., and Glass, J. B. (2011) The geochemical record of the ancient nitrogen cycle, nitrogen isotopes, and metal cofactors. *In* "Methods in Enzymology," Vol. 486, pp. 483-506.

Grasby, S. E., Beauchamp, B., and Knies, J. (2016) Early Triassic productivity crises delayed recovery from world's worst mass extinction. GSA, Vol. 44, pp. 779-782.

Grasby, S. E., Beauchamp, B. P.G., Wignall, P., Talavera, C., Galloway, J. M., Piepjohn, K., Reinhardt, L., and Blomeier, D. (2015) Progressive environmental deterioration in the northwestern Pangea leading to the latest Permian extinction. GSA Bulletin, Vol. 127, pp. 1331-1347.

Hoefs, Jochen. (2015) Stable isotope geochemistry. Springer, Berlin, pp. 1-402.

Holbourn, A., Kuhnt, W., Schulz, M., Flores, J. A. and Anderson, N. (2007) Orbitally-paced climate evolution during the middle Miocene "Monterey" carbon isotope excursion. Earth and Planetary Science Letters. Vol. 261, pp. 534-550.

Jenkyns, H. C., Gröcke, D. R., and Hesselbo, S. P. (2001) Nitrogen isotope evidence for water mass denitrification during the early Toarcian (Jurassic) oceanic anoxic event. Paleoceanography, Vol. 16, pp. 593-603.

Junium, C. K., and Arthur, M. A. (2007) Nitrogen cycling during the Cretaceous, Cenomanian-Turonian Oceanic Anoxic Event II. Geochemistry, Geophysics, Geosystems, Vol. 8, p. Q03002.

Kern, M., Watzinger, A., and Scherr, K. E. (2016) ^{15}N-nitrate and ^{34}S-sulfate isotope fractionation reflects electron acceptor 'recycling' during hydrocarbon biodegradation. New Biotechnology, In Press.

Kikumoto, R., Tahata, M., Nishizawa, M., Sawaki, Y., Maruyama, S., Shu, D., Han, J., Komiya, T., Takai, K., and Ueno, Y. (2014) Nitrogen isotope chemostratigraphy of the Ediacaran and Early Cambrian platform sequence at Three Gorges, South China. Gondwana Research, Vol. 25, pp. 1057-1069.

Knies, J., Brookes, S., and Schubert, C. J. (2007) Re-assessing the nitrogen signal in continental margin sediments: New insights from the high northern latitudes. Earth and Planetary Science Letters, Vol. 253, pp. 471-484.

Knies, J., Grasby, S. E., Beauchamp, B., and Schubert, C. J. (2013) Water mass denitrification during the latest Permian extinction in the Sverdrup Basin, Arctic Canada. Geology, Vol. 41, pp. 167-170.

Kritee, K., Sigman, D. M., Granger, J., Ward, B. B., Jayakumar, A., and Deutsch, C. (2012) Reduced isotope fractionation by denitrification under conditions relevant to the ocean. Geochimica et Cosmochimica Acta, Vol. 92, pp. 243-259.

Kuypers, M. M. M., van Breugel, Y., Schouten, S., Erba, E., and Damsté, J. S. S. (2004) N2-fixing cyanobacteria supplied nutrient N for Cretaceous oceanic anoxic events. Geology, Vol. 32, pp. 853-856.

Lam, P., Lavik, G., Jensen, M. M., van de Vossenberg, J., Schmid, M., Woebken, D., Gutiérrez, D., Amann, R., Jetten, M. S. M., and Kuypers, M. M. M. (2009) Revising the nitrogen cycle in the Peruvian oxygen minimum zone. Proc. Natl. Acad. Sci. USA, Vol. 106, pp. 4752-4757

Lehmann, Moritz F., Bernasconi, Stefano M., Barbieri, Alberto., and McKenzie, Judith A. (2002) Preservation of organic matter and alteration of its carbon and nitrogen isotope composition during simulated and in situ early sedimentary diagenesis. Geochimica et Cosmochimica Acta, Vol. 66, pp. 3573-3584.

Levman, B. G. and von Bitter, P. H. (2002) The Frasnian-Famennian (mid-Late Devonian) boundary in the type section of the Long Rapids Formation, James Bay Lowlands, northern Ontario, Canada. Canada Journal of Earth Science, Vol. 39, pp. 1795-1818.

Liao, Y., Geng, A., and Huang, H. (2009) The influence of biodegradation on resins and asphaltenes in the Liaohe Basin. Organic Geochemistry, Vol. 40, pp. 312-320.

Liu, J., Qie, W., Algeo, T. J., Yao, L., Huang, J., and Luo, G. (2016) Changes in marine nitrogen fixation and denitrification rates during the end-Devonian mass extinction. Palaeogeography, Palaeoclimatology, Palaeoecology, Vol. 448, pp. 195-206.

Luo, G., Wang, Y., Algeo, T. J., Kump, L. R., Bia, X., Yang, H., Yao, L., and Xie, S. (2011) Enhanced nitrogen fixation in the immediate aftermath of the latest Permian marine mass extinction. Geolgy, Vol. 39, pp. 647-650.

Luo, G., Algeo, T. J., Zhan, R., Yan, D., Huang, J., Liu, J., and Xie, S. (2016) Perturbation of the marine nitrogen cycle during the Late Ordovician glaciation and mass extinction. Palaeogeography, Palaeoclimatology, Palaeoecology, Vol. 448, pp. 339-348.

Macko, S. A., and Quick, R. S. (1986) A geochemical study of oil migration at source rock reservoir contacts: Stable isotopes. Organic geochemistry, Vol. 10, pp. 199-205.

Macko, S. A., and Pereira, C. P. G. (1990) Neogene paleoclimate development of the Antarctic Weddell Sea region: organic geochemistry. Proceedings of the Ocean Drilling Program, Scientific Results, Vol. 113, pp. 881-897.

Majewski, W., and Bohaty, S. M. (2010) Surface-water cooling and salinity decrease during the Middle Miocene climate transition at Southern Ocean ODP Site 747 (Kerguelen Plateau). Marine Micropaleontology, Vol. 74, pp. 1-14.

Marcano, N., Larter, S., and Mayer, B. (2013) The impact of severe biodegradation on the molecular and stable (C, H, N, S) isotopic compositions of oils in the Alberta Basin, Canada. Organic Geochemistry, Vol. 59, pp. 114-132.

Marty, B., Zimmermann, L., Pujol, M., Burgess, R., Philippot, P. (2013) Nitrogen isotopic composition and density of the Archean atmosphere. Science, Vol. 342, pp. 101-104.

Meckler, A. N., Ren, H., and Sigman, D. M. Gruber, N., Plessen, B., Schubert, C.J., and Haug, G. (2011) Deglacial nitrogen isotope changes in the Gulf of Mexico: Evidence from bulk sedimentary and foraminifera-bond nitrogen in Orca Basin sediments. Paleoceanography, Vol. 26, PA4216, doi:10.1029/2011PA002156.

Melchin, M. J., Mitchell, C. E., Holmden, C., and Štorch, P. (2013) Environmental changes in the Late Ordovicain-early Silurian: Review and new insights from black shales and nitrogen isotopes. GSA Bulletin, Vol. 125, pp. 1635-1670.

Mizukami, T., Kaiho, K., and Oba, M. (2013) Significant changes in land vegetation and oceanic redox across the Cretaceous/Paleogene boundary. Palaeogeography, Palaeoclimatology, Palaeoecology, Vol. 369, pp. 41-47.

Möbius,J., Gaye, B., Lahajnar, N., Bahlmann, E., and Emeis, K. (2011) Influence of diagenesis on sedimentary $\delta^{15}N$ in the Arabian Sea over the last 130 kyr. Marine Geology, Vol. 284, pp. 127-138.

Mulder, A., van de Graaf, A. A., Robertson, L. A., and Kuenen, J. G. (1995) Anaerobic ammonium oxidation discovered in a denitrifying fluidized bed reactor. FEMS Microbiology Ecology, Vol. 16, pp. 177-184.

Núñez-Useche, F., Canet, C., Barragán, R., and Alfonso, P. (2016) Bioevents and redox conditions around the Cenomanian-Turonian anoxic event in Central Mexico. Palaeogeography, Palaeoclimatology, Palaeoecology, Vol. 449, pp. 205-226.

Oldenburg, T. B. P., Larter, S. R., and Huang, H. (2007) Nitrogen isotope systematics of petroleum fractions of differing polarity- Neutral versus basic compounds. Organic Geochemistry, Vol. 38, pp. 1789-1794.

Paul, D., Skrzypek, G., Forizs, I. (2007) Normalization of measured stable isotopic compositions to isotope reference scales- a review. Rapid Commun. Mass Spectrom. Vol. 21, pp. 3006-3014.

Peters, K. E., Walters, C. C., and Moldowan, J. M. (2005) The Biomarker Guide. (2nd edition) Cambridge University Press.

Qi, H., Coplen,T.B., Geilmann, H., Bland, W.A., Bohlke, J.K. (2003) Two new organic reference materials for $\delta^{13}C$ and $\delta^{15}N$ measurements and a new value for the $\delta^{13}C$ of NBS 22 oil. Rapid Commun. Mass Spectrom. Vol. 17, pp. 2483-2487.

Quan, T. M., Adigwe, E. N., Riedinger, N., and Puckette, J. (2013) Evaluating nitrogen isotopes as proxies for depositional environmental conditions in shales: Comparing Caney and Woodford Shales, Anadarko Basin, Oklahoma, USA. Chemical Geology, Vol. 360-361, pp. 231-240.

Rau, G. H., Arthur, M. A., and Dean, W. (1987) $^{15}N/^{14}N$ variations in Cretaceous Atlantic sedimentary sequences: implication for past changes in marine nitrogen biochemistry. Earth and Planetary Science Letters, Vol. 82, pp. 269-279.

Rivera, K. T. (2013) Geologic controls on nitrogen isotopes in marine black shale: A case study of the Woodford shale, Anadarko basin, Oklahoma. MS Thesis, Oklahoma State University, pp. 1-141.

Rivera, K. T., Puckette, J. and Quan, T. M. (2015) Critical evaluation of redox verse thermal maturity controls on 15N in organic-rich shales: A case study of the Woodford Shale, Anadarko Basin, Oklahoma, USA. Organic Geochemistry, Vol. 83-84, pp. 127-139.

Robinson, R., Kienast, M., Albuquerque, A. L., and Altabet, S. C. (2012) A review of nitrogen isotopic alteration in marine sediments. Paleoceanography, Vol. 27, PA4203, doi:10.1029/2012PA002321.

Saitoh, M., Ueno, Y., Nishizawa, M., Isozaki, Y., Takai, K., Yao, J., Ji, Z. (2014) Nitrogen isotope chemostratigraphy across the Permian-Triassic boundary at Chaotian, Sichuan, South China. Journal of Asian Earth Sciences, Vol. 93, pp. 113-128.

Saltzman, M. R. (2002) Carbon and oxygen isotope stratigraphy of the Lower Mississippian (Kinderhookian-lower Osagean), western United States: implications for seawater chemistry and glaciation. GSA Bulletin, Vol. 114, pp. 96-108.

Schimmelmann, A., and Lis, G. P. (2010) Nitrogen isotopic exchange during maturation of organic matter. Organic Geochemistry, Vol. 41, pp. 63-70.

Schoepfer, S. D., Henderson, C. M., Garrison, G. H., and Ward, P. D. (2012) Cessation of a productive coastal upwelling system in the Panthalassic Ocean at the Permian-Triassic Boundary. Palaeogeography, Palaeoclimatology, Palaeoecology, Vol. 313-314, pp. 181-188.

Schoepfer, S. D., Algeo, T. J., Ward, P. D., Williford, K. H. and Haggart, J. W. (2016) Testing the limits in a greenhouse ocean: Did low nitrogen availability limit marine productivity during the end-Triassic mass extinction? Earth and Planetary Science Letters, Vol. 451, pp. 138-148.

Sheehan, P. M. (2001) The Late Ordovician Mass Extinction. Annual Review of Earth and Planetary Sciences, Vol. 291, pp. 331-364.

Sigman, D. M., and Casciotti, K. L. (2001) Nitrogen isotopes in the ocean. *In* "Encyclopedia of Ocean Sciences," (Second Edition) pp. 40-54.

Snowdon, L. R., Volkman, J. K., Zhang, Z., Tao, G., and Liu, P. (2016) The organic geochemistry of asphaltenes and occluded biomarkers. Organic Geochemistry, Vol. 91, pp. 3-15.

Sepúlveda, J., Wendler, J. E., Summons, R. E., and Hinrichs, K. (2009) Rapid Resurgence of marine productivity after the Cretaceous-Paleogene mass extinction. Science, Vol. 326, pp. 129-132.

Strąpoć, D., Mastalerz, M., Schimmelmann, A., Drobniak, A., and Hasenmueller, N. R. (2010) Geochemical constrainsts on the origin and volume of gas in the New Albany Shale, (Devonian-Mississippian), eastern Illinois Basin. AAPG Bulletin, Vol. 94, pp. 1713-1740.

Stüeken, E. E., Buick, R., Guy, B. M., and Koehler, M. C. (2015) Isotopic evidence for biological nitrogen fixation by molybdenum-nitrogenase from 3.2 Gyr. Nature, Vol. 520, pp. 666-669.

Sun, Y., Joachimski, M. M., Wignall, P. B., Yan, C., Chen, Y., Jiang, H., Wang, L., and Lai, X. (2012) Lethally hot temperatures during the Early Triassic greenhouse. Science, Vol. 338, pp. 366-370.

Tesdal, J. E., Galbraith, E. D., and Kienast, M. (2013) Nitrogen isotopes in bulk marine sediment: linking seafloor observations with subseafloor records. Biosciences, Vol. 10, pp. 101-118.

Vandenbroucke, M., and Largeau, C. (2007) Kerogen origin, evolution and structure. (2007) Organic Geochemistry, Vol. 38, pp. 719-833.

Verducci, M., Foresi, L. M., Scott, G. H., Sprovieri, M., Lirer, F., and Pelosi, N. (2009) The Middle Miocene climatic transition in the Southern Ocean: Evidence of paleoclimate and hydrographic changes at Kerguelen plateau from planktonic foraminifers and stable isotopes. Palaeogeography, Palaeoclimatology, Palaeoecology, Vol. 280, pp. 371-386.

Wallace, Z. A., and Elrick, M. (2014) Early Mississippian orbital-scale glacio-eustasy detected from high-resolution oxygen isotopes of marine apatite. Journal of Sedimentary Research, Vol. 84, pp. 816-824.

Wang, D., Struck, U., Ling, H. F., Guo, Q. J., Shields-Zhou, G. A., Zhu, M. Y., and Yao, S. P. (2015) Marine redox variations and nitrogen cycle of the early Cambrian southern margin of the Yangtze Platform, South China: Evidence from nitrogen and organic carbon isotopes. Precambrian Research, Vol. 267, pp. 209-226.

Wenk, C. B. (2013) Nitrogen transformation pathways, rates and isotopic signatures in Lake Lugano. Ph.D. thesis, Department of Environmental Sciences, University of Basel, Switzerland, pp. 1-136.

Williams, Lynda B., Ferrell Jr., Ray E., Hutcheon, Ian., Bakel, Allen J., Walsh, Maud M., and Krouse, H. Roy. (1995) Nitrogen isotope geochemistry of organic matter and minerals during diagenesis and hydrocarbon migration. Geochimica et Cosmochimica Acta, Vol. 59, pp. 765-779.

Zhang, T., Shen, Y., Zhan, R., Shen, S., and Chen, X. (2009) Large perturbations of the carbon and sulfur cycle associated with the Late Ordovician mass extinction in South China. Geology, Vol. 37, pp. 299-302.

Zhou, L., Algeo, T. J., Shen, J., Hu, Z., Gong, H., Xie, S., Huang, J., and Gao, S. (2015) Changes in marine productivity and redox conditions during the Late Ordovician Hirnantian glaciation. Palaeogeography, Palaeoclimatology, Palaeoecology, Vol. 420, pp. 223-234.

Appendix 1: Age, lithology, and sample location

Sample ID	GeoMark Lab ID	Geologic Age of Source Rocks	Lithology/Depositional Environment	Sample Location
1	CA-0022	Neogene	Distal Marine Shale	San Joaquin Basin, US
2	CA-0024	Neogene	Distal Marine Shale	San Joaquin Basin, US
3	PH-0031	Neogene	Marine Carbonate	Palawan Shelf, Philippines
4	RU-0411	Neogene	Distal Marine Shale	North Sakhalin Basin, Russia
5	PL-0002	Paleogene	Distal Marine Shale	North Carpathian Basin, Poland
6	IN-0084	Paleogene	Distal Marine Shale	Zagros Fold Belt, Iran
7	HU-0004	Paleogene	Distal Marine Shale	Pannonian Basin, Hungary
8	VA-0052	Upper Cretaceous	Marine Carbonate	Maracaibo Basin, Venezuela
9	EC-0084	Upper Cretaceous	Marine Marl	Putumayo-Oriente-Maranon Basin, Equador
10	WY-0475	Upper Cretaceous	Distal Marine Shale	Powder River Basin, US
11	LI-0060	Upper Cretaceous	Distal Marine Shale	Sirte Basin, Libya
12	PR-0055	Upper Cretaceous	Distal Marine Shale/ Marine Marl	Putumayo-Oriente-Maranon Basin, Peru
13	CO-0031	Upper Cretaceous	Marine Carbonate	West-Central Cordillera, Colombia
14	TX-1828	Upper Cretaceous	Distal Marine Shale/ Marine Marl	Western Gulf, US
15	TX-1855	Upper Cretaceous	Distal Marine Shale- Eagle Ford/ Dexter Mix	East Texas Basin, US
16	IN-0009	Lower Cretaceous	Marine Marl	Zagros Fold Belt, Iran
17	WY-0695	Lower Cretaceous	Distal Marine Shale	Powder River Basin, US
18	TX-0120	Lower Cretaceous	Distal Marine Shale/ Marine Marl	East Texas Basin, US
19	FL-0002	Lower Cretaceous	Marine Carbonate	Florida Peninsula, US
20	IA-0010	Lower Cretaceous	Distal Marine Shale	Cauvery, India
21	SA-0063	Upper Jurassic/Lower Cretaceous	Marine Carbonate	Mesopotamian Foredeep Basin, Kuwait
22	MX-0087	Upper Jurassic/Lower Cretaceous	Marine Carbonate	Tampico-Misantla Basin, Mexico

23	KW-0003	Upper Jurassic/Lower Cretaceous	Marine Carbonate	Mesopotamian Foredeep Basin, Saudi Arabia
24	RU-0119	Upper Jurassic	Distal Marine Shale	West Siberian Basin, Russia
25	SA-0051	Upper Jurassic	Marine Carbonate	Greater Ghawar Uplift, Saudi Arabia
26	SA-0123	Upper Jurassic	Marine Carbonate	Greater Ghawar Uplift, Saudi Arabia
27	SA-0129	Upper Jurassic	Marine Carbonate	Greater Ghawar Uplift, Saudi Arabia
28	UK-0051	Upper Jurassic	Distal Marine Shale	North Sea Graben, UK
29	CN-0138	Upper Jurassic	Distal Marine Shale	Labrador-Newfoundland Shelf, Canada
30	MX-0024	Upper Jurassic	Marine Carbonate	Villahermosa Uplift, Mexico
31	MX-0067	Upper Jurassic	Marine Carbonate	Saline-Comalcalco Basin, Mexico
32	MX-0078	Upper Jurassic	Marine Carbonate	Chiapas Massif-Nuclear Central America, Mexico
33	MX-0137	Upper Jurassic	Marine Carbonate	Saline-Comalcalco Basin, Mexico
34	MX-0018	Upper Jurassic	Marine Marl	Saline-Comalcalco Basin, Mexico
35	SA-0006	Upper Jurassic	Marine Carbonate	Mesopotamian Foredeep Basin, Saudi Arabia
36	AS-0261	Lower-Middle Jurassic	Distal Marine Shale	Cook Inlet OCS, US
37	FR-0014	Lower-Middle Jurassic	Distal Marine Shale	Anglo-Paris Basin, France
38	AS-0118	Triassic	Marine Carbonate	Beaufort Shelf OC, US
39	SY-0051	Triassic	Marine Marl	Haleb, Syria
40	AR-0230	Triassic	Lacustrine Fresh	Cuyo Basin, Argentina
41	SI-0010	Triassic	Hypersaline-Restricted	Sicily, Italy
42	NM-0059	Permian	Marine Marl	Permian Basin, US
43	WY-0666	Permian	Marine Carbonate	Big Horn Basin, US
44	NM-0120	Permian	Marine Carbonate	Permian Basin, Us
45	TX-1224	Permian	Marine Marl	Palo Duro Basin, US
46	NM-0345	Permian	Marine Carbonate	Permian Basin, US
47	TX-1845	Permian	Hypersaline-Restricted	Anadarko Basin, US

48	NM-0149	Lower Permian	Marine Distal Shale- Wolfcamp Fm.	Permian Basin, US
49	NM-0192	Lower Permian	Marine Distal Shale- Wolfcamp Fm.	Permian Basin, US
50	TX-1809	Upper Pennsylvanian	Distal Marine Shale- Cline Fm	Permian Basin, US
51	TX-0706	Carboniferous	Distal Marine Shale	Bend Arch- Fort Worth Basin, US
52	TX-1639	Upper Mississippian	Distal Marine Shale	Montague Co. TX, US
53	OK-0046	Upper Devonian/ Lower Mississippian	Distal Marine Shale-Woodford Fm.	Southern Oklahoma, US
54	KY-0014	Devonian	Distal Marine Shale	Cincinnati Arch, US
55	ND-0267	Upper Devonian/ Lower Mississippian	Distal Marine Shale	Williston Basin, US
56	CN-0044	Devonian	Marine Marl	Alberta Basin, Canada
57	RU-0354	Devonian	Marine Carbonate	Volga-Ural Region, Russia
58	SW-0001	Ordovician/Silurian	Distal Marine Shale	Baltic Depression, Sweden
59	MI-0069	Silurian	Marine Carbonate/Hypersaline-Restricted	Michigan Basin, US
60	TX-1018	Ordovician	Distal Marine Shale	Permian Basin, US
61	OM-0059	Precambrian/Cambrian	Distal Marine Shale/ Marine Marl	Fahud Salt Basin, Oman
62	OM-0012	Precambrian/Cambrian	Marine Marl	South Oman Salt Basin, Oman

Appendix 2: Age and $\delta^{15}N$ values for the for each oil sample

Sample ID	Geologic Age of Source Rocks	$\delta^{15}N$ ‰ (NSO)	$\delta^{15}N$ ‰ (Asp)
1	Neogene	7.92 ± 0.57	7.44 ± 0.39
2	Neogene	6.20 ± 0.13	5.61 ± 1.22
3	Neogene	1.23 ± 0.45	0.96 ± 0.23
4	Neogene	3.04 ± 0.69	4.22 ± 0.45
5	Paleogene	0.07 ± 0.30	0.96 ± 0.44
6	Paleogene	1.78 ± 1.10	2.2 1± 0.11
7	Paleogene	2.18 ± 0.72	2.10 ± 0.51
8	Upper Cretaceous	2.06 ± 0.05	1.74 ± 0.16
9	Upper Cretaceous	1.62 ± 0.52	1.36 ± 0.41
10	Upper Cretaceous	-1.60 ± 0.64	-0.52 ± 0.25
11	Upper Cretaceous	5.42 ± 0.41	5.35
12	Upper Cretaceous	1.44 ± 0.67	1.71 ± 0.88
13	Upper Cretaceous	3.50 ± 0.37	2.38 ± 0.87
14	Upper Cretaceous	-0.06 ± 0.10	-0.09 ± 0.32
15	Upper Cretaceous	-0.24 ± 0.37	0.09 ± 0.36
16	Lower Cretaceous	1.17 ± 0.04	0.02 ± 0.05
17	Lower Cretaceous	0.80 ± 0.17	1.28 ± 0.54
18	Lower Cretaceous	-0.23 ± 0.13	-0.26
19	Lower Cretaceous	-0.25 ± 0.04	1.40 ± 0.40
20	Lower Cretaceous	-0.37 ± 0.47	1.24 ± 0.01
21	Upper Jurassic/Lower Cretaceous	0.59 ± 1.13	0.51 ± 0.82
22	Upper Jurassic/Lower Cretaceous	0.20 ± 0.19	-0.80 ± 0.23
23	Upper Jurassic/Lower Cretaceous	1.45 ± 0.78	1.05 ± 0.44
24	Upper Jurassic	-0.25 ± 0.59	-0.33 ± 0.35
25	Upper Jurassic	1.20 ± 0.61	2.20 ± 0.41
26	Upper Jurassic	1.91 ± 0.64	2.40 ± 0.44

27	Upper Jurassic	0.59 ± 0.50	1.46 ± 0.33
28	Upper Jurassic	1.74 ± 0.01	1.20 ± 0.17
29	Upper Jurassic	1.14 ± 0.23	0.82 ± 0.03
30	Upper Jurassic	1.24 ± 0.87	-0.70 ± 0.61
31	Upper Jurassic	0.65 ± 0.97	-0.34 ± 0.21
32	Upper Jurassic	0.70 ± 0.81	0.17 ± 0.32
33	Upper Jurassic	-0.87 ± 0.60	-0.92 ± 0.42
34	Upper Jurassic	0.39 ± 0.50	0.04 ± 0.15
35	Upper Jurassic	1.51 ± 0.33	2.65 ± 0.69
36	Lower-Middle Jurassic	1.11 ± 0.62	0.44 ± 0.48
37	Lower-Middle Jurassic	0.79 ± 0.34	0.82 ± 0.43
38	Triassic	6.48 ± 0.78	7.12 ± 0.62
39	Triassic	2.0 ± 0.23	1.88 ± 0.35
40	Triassic	5.04 ± 0.12	3.20 ± 0.49
41	Triassic	5.43 ± 0.22	5.30 ± 0.91
42	Permian	11.49 ± 0.86	12.71 ± 0.56
43	Permian	13.32 ± 0.53	16.00 ± 1.08
44	Permian	6.24 ± 1.11	6.70 ± 0.30
45	Permian	9.23 ± 0.24	11.32 ± 0.62
46	Permian	8.73 ± 1.02	9.40 ± 1.55
47	Permian	4.78 ± 0.33	1.53
48	Lower Permian	8.33 ± 0.53	9.68 ± 0.89
49	Lower Permian	11.93 ± 0.25	12.27 ± 0.34
50	Upper Pennsylvanian	15.57 ± 0.20	
51	Carboniferous	3.93 ± 0.78	3.26 ± 0.73
52	Upper Mississippian	9.72 ± 0.44	
53	Upper Devonian/ Lower Mississippian	0.87 ± 0.21	0.67 ± 0.24
54	Devonian	-0.68 ± 0.54	1.76 ± 0.36
55	Upper Devonian/ Lower Mississippian	0.45 ± 0.33	
56	Devonian	0.14 ± 0.82	0.24 ± 0.12

57	Devonian	-0.26 ± 0.56	-0.20 ± 0.20
58	Ordovician/Silurian	-0.93 ± 0.38	-1.30 ± 0.36
59	Silurian	2.40 ± 1.30	0.54
60	Ordovician	5.60 ± 0.45	3.68 ± 0.67
61	Precambrian/Cambrian	2.61 ± 0.72	2.83 ± 0.18
62	Precambrian/Cambrian	3.88 ± 0.53	2.38 ± 0.27